ROYAL SOCIETY OPEN SCIENCE

rsos.royalsocietypublishing.org

Research

Cite this article: Yu T, Ma Y-D, Lai W-P, Liu Y-Z, Ge Z-X, Ren G. 2018 Roads to pentazolate anion: a theoretical insight. *R. Soc. open sci.* **5**: 172269.
http://dx.doi.org/10.1098/rsos.172269

Received: 3 January 2018
Accepted: 18 April 2018

Subject Category:
Chemistry

Subject Areas:
computational chemistry/inorganic chemistry/physical chemistry

Keywords:
potential energy surface, reaction mechanism, polynitrogen, pentazole

Author for correspondence:
Tao Yu
e-mail: fischer@wo.cn

This article has been edited by the Royal Society of Chemistry, including the commissioning, peer review process and editorial aspects up to the point of acceptance.

Electronic supplementary material is available online at https://dx.doi.org/10.6084/m9.figshare.c.4096412.

THE ROYAL SOCIETY PUBLISHING

Roads to pentazolate anion: a theoretical insight

Tao Yu, Yi-Ding Ma, Wei-Peng Lai, Ying-Zhe Liu, Zhong-Xue Ge and Gan Ren

State Key Laboratory of Fluorine and Nitrogen Chemicals, Xi'an Modern Chemistry Research Institute, Xi'an, People's Republic of China

TY, 0000-0001-9516-4259

The formation mechanism of pentazolate anion (PZA) is not yet clear. In order to present the possible formation pathways of PZA, the potential energy surfaces of phenylpentazole (PPZ), phenylpentazole radical (PPZ-R), phenylpentazole radical anion (PPZ-RA), PPZ and *m*-chloroperbenzoic acid (*m*-CPBA), *p*-pentazolylphenolate anion (*p*-PZPolA) and *m*-CPBA, and *p*-pentazolylphenol (*p*-PZPol) and *m*-CPBA were calculated by the computational electronic structure methods including the hybrid density functional, the double hybrid density functional and the coupled-cluster theories. At the thermodynamic point of view, the cleavages of C–N bonds of PPZ and PPZ-R need to absorb large amounts of heat. Thus, they are not feasible entrance for PZA formation at ambient condition. But excitation of PPZ and deprotonation of PPZ-RA probably happen before cleavage of C–N bond of PPZ at high-energy condition. As to the radical anion mechanism, the high accuracy calculations surveyed that the barrier of PZA formation is probably lower than that of dinitrogen evolution, but the small ionization potential of PPZ-RA gives rise to the unstable ionic pair of sodium PPZ at high temperature. In respect of oxidation mechanism, except for PPZ, the reactions of *p*-PZPolA and *p*-PZPol with *m*-CPBA can form PZA and quinone. The PZA formations have the barriers of about 20 kcal mol^{-1} which compete with the dinitrogen evolutions. The stabilities of PZA in both solid and gas phases were also studied herein. The proton prefers to transfer to pentazolyl group in the $(N_5)_6(H_3O)_3(NH_4)_4Cl$ system which leads to the dissociation of pentazole ring. The ground states of $M(N_5)_2(H_2O)_4$ (M = Co, Fe and Mn) are high-spin states. The pentazolyl groups confined by the crystal waters in the coordinate compounds can improve the kinetic stability. As to the reactivity of PZA, it can be persistently oxidized by *m*-CPBA to oxo-PZA and 1,3-oxo-PZA with the barriers of about 20 kcal mol^{-1}.

1. Introduction

Nitrogen is located at the second period and group 15 of the element table. The standard state manifests as a diatomic gas

with a formula of N_2. Owing to the highly strong triple bond, it imparts a low chemical reactivity. By contrast to formation, the combustion or decomposition of a nitrogenous compound ultimately releases dinitrogen following the thermodynamics. Consequently, the homopolyatomic states of nitrogen are metastable with high energy. Although they are difficult to synthesize, the innovation of the element chemistry and the exploration of the stable margin have been attractive to the science community, and the promising applications on the space, defence and oil drilling technologies have been interesting to the engineering community.

Since azide anion [1] (N_3^-) and pentazenium cation [2] (N_5^+) were discovered, pentazolate anion (N_5^-) had been expected to be the third homopolynitrogen species in bulk based on the successful synthesis of arylpentazoles [3]. Some high-level calculations indicated that the dissociation barrier towards N_3^- and N_2 exceeds 25 kcal mol^{-1}, e.g. 26 kcal mol^{-1} at CASPT2/ANO(4s3p2d) level by Curtiss *et al.* [4], 27.7 kcal mol^{-1} at CCSD(T)/aug-cc-pVTZ level by Nguyen & Ha [5], and 27.2 kcal mol^{-1} at CCSD(T)/CBS level by Dixon *et al.* [6]. The sufficient barrier makes pentazolate anion (PZA) possible to be held at ambient condition. Over time, PZA was only detected in spectrum as to the experimental attempts. Vij *et al.* [7] in 2002 observed the *m/z* 70 (71 for a pentazole ring containing one ^{15}N) peak of mass spectrometry using electrospray ionization (ESI) at high collision voltages for *p*-pentazolylphenolate anion (*p*-PZPolA). The removal of aryl group of *p*-PZPolA undergoes an intersystem crossing between singlet and triplet states with a barrier of 63.8 kcal mol^{-1} at the CASSCF(12,11)/DZV level [8]. Östmark *et al.* [9] in 2003 also discovered the peak of mass spectrometry using a relatively mild ionization, i.e. UV-laser desorption ionization (LDI), for *p*-dimethylaminophenylpentazole. Although the starting material also contains the arylpentazolyl structure, *p*-dimethylaminophenylpentazole forms PZA in a different pathway. The cleavage of the C–N bond has a radical anion mechanism with a barrier of 21.1 kcal mol^{-1} at the B3LYP/6-311+(2df,p) level [9]. However, ESI and UV-LDI methods cannot keep PZA a long life. Bazanov *et al.* [10] in 2016 treated phenylpentazole (PPZ) with sodium in tetrahydrofuran (THF), and the mass spectrometry of PZA was detected with an elution time of 2.1 min after injection into the HPLC column. The electron transfer from sodium to PPZ also follows the radical anion mechanism [11]. The cleavage of the C–N bond competes with the evolution of dinitrogen. Their ^{15}N labelled experiment further substantiated the discovery of PZA in solution in 2017 [12]. The detection of PZA in an extreme condition reported by Steele *et al.* [13] in 2017 is the phase change for mixture of caesium azide and liquid dinitrogen in a diamond anvil cell (DAC) at a super high pressure near 60 GPa. The existence of PZA was supported by XRD, Raman and computational studies, but the PZA disappeared when the external pressure was relieved [13]. Laniel *et al.* [14] in 2018 observed PZA in DAC around 45 GPa using lithium embedded in dinitrogen. The Raman modes and *m/z* 70 peak of mass spectrometry for PZA could still be measured at ambient condition which means LiN_5 is metastable [14]. As to the chemical synthesis ways, the redox reactions were designed for the cleavage of C–N bond of *p*-pentazolylphenol (*p*-PZPol) derivatives. Butler *et al*. [15] in 2003 claimed that PZA was identified by NMR spectroscopy using the oxidizer of cerium ammonium nitrate. The discovery was argued by Schroer *et al*. [16] in 2005. The reinvestigation of Butler *et al*. [17] in 2008 still did not find the direct evidence on PZA. Although the computational result of Perera *et al*. [18] in 2009 for the spin–spin constants of ^{15}N–^{15}N supported the observation of Butler in 2003. Most recently, there has been breakthrough in 2017 for the synthesis of PZA in bulk. Zhang *et al.* [19] managed to cleave PZA out of 3,5-dimethyl-4-hydroxyphenylpentazole through treatment with *m*-chloroperbenzoic acid (*m*-CPBA) and ferrous bisglycinate and successfully isolated a stable salt of $(N_5)_6(H_3O)_3(NH_4)_4Cl$ in the crystalline state with a decomposition onset temperature of 117°C. Afterwards they obtained the crystal structure of $Co(N_5)_2(H_2O)_4{\cdot}4H_2O$ [20]. Likewise based on $(N_5)_6(H_3O)_3(NH_4)_4Cl$, the three-dimensional frameworks with the formulae of $N_{80}Na_{15.33}O_5$ and $[Ag(NH_3)_2]^+[Ag_3(N_5)_4]^-$ were synthesized by Zhang *et al.* [21] and Sun *et al.* [22] in 2018, respectively. Xu *et al.* [23] in 2017 used almost the same approach, but obtained a different crystal with a formula of $Na(N_5)(H_2O){\cdot}2H_2O$. Based on the sodium pentazolate hydrate, a series of metal salts including $M(N_5)_2(H_2O)_4{\cdot}4H_2O$ (M = Fe and Mn) and $Mg(H_2O)_6(N_5)_2{\cdot}4H_2O$ were synthesized. Afterwards they synthesized three anhydrous and metal-free salts including $(N_5^-)_2DABTT^{2+}$ (DABTT = 3,9-diamino-6,7-dihydro-5*H*-bis([1,2,4]triazolo)[4,3-e:3′,4′-g][1,2,4,5] tetrazepine-2,10-diium), $N_5^-GU^+$ (GU = *N*-carbamoylguanidinium) and $N_5^-Oxahy^+$ (Oxahy = oxalohydrazinium) [24].

Since the successful synthesis of N_5^+ in 1999 [2], the formation mechanisms for $N_2F^+ + HN_3$ [25,26] and $ONF_2^+ + HN_3$ [26–28] had been thoroughly expounded by the aids of theoretical and computational chemistry. Although the great advances of PZA have been made, there are still questions regarding the mechanisms on its formation and stabilization. Thus, the computational tasks on the reaction pathways for the high-energy, radical anion and redox methods were put forward. Our investigations include the following contents: the potential energy surface (PES) scans around PPZ, PPZ-R (phenylpentazole

radical), PPZ-RA (phenylpentazole radical anion), PPZ and *m*-CPBA, *p*-PZPolA and *m*-CPBA, *p*-PZPol and *m*-CPBA and $M(N_5)_2(H_2O)_4$ (M = Co, Fe and Mn), and the evaluations of PZA stabilities in both isolated and condensed states. The computational results are expected to be useful for deeply understanding the characteristics of PZA, and tutoring the design and synthesis of the high-energy compounds comprising PZA in the future works.

2. Computational methods

2.1. Quantum chemistry

The total electronic energies of the isolated states were calculated by the B3LYP [29,30] (a hybrid density functional), RI-B2KPLYP (a double hybrid density functional with the kinetic reparametrization [31] of B2PLYP [32] and RI approximation [33] used for the second-order many-body perturbation part) and CCSD(T) [34–38] (coupled-cluster singles and doubles with perturbative triples) methods. The basis set of 6-311++G** for CHNO elements [39] and effective core potential of LanL2 with valence basis set of LanLDZ for CoFeMn elements [40,41] were used to express the wave functions of the B3LYP method. The basis set of ma-def2-TZVP [42,43] (the auxiliary basis of RI approximation was automatically constructed) was used to combine with the RI-B2KPLYP method. Based on the geometries optimized at the B3LYP/6-311++G** level, the complete basis set (CBS) was used to combine with the frozen core CCSD(T) method. The basis set extrapolation [44] for CBS deduced by cc-pVDZ [45] and cc-pVTZ [45] was divided into the Hartree–Fock (HF) and correlated parts. Using the different converged approaches of two parts, the small basis sets can efficiently get to the complete limit. The specific equation on the total electronic energy calculated at the CCSD(T)/CBS level is presented as follows:

$$E_{\mathrm{CBS}}^{\mathrm{CCSD(T)}} = \frac{3^{3.4}}{3^{3.4}-2^{3.4}}E_{\mathrm{cc-pVTZ}}^{\mathrm{HF}} - \frac{2^{3.4}}{3^{3.4}-2^{3.4}}E_{\mathrm{cc-pVDZ}}^{\mathrm{HF}} + \frac{3^{2.4}}{3^{2.4}-2^{2.4}}(E_{\mathrm{cc-pVTZ}}^{\mathrm{CCSD}(T)} - E_{\mathrm{cc-pVTZ}}^{\mathrm{HF}}) - \frac{2^{2.4}}{3^{2.4}-2^{2.4}}(E_{\mathrm{cc-pVDZ}}^{\mathrm{CCSD}(T)} - E_{\mathrm{cc-pVDZ}}^{\mathrm{HF}}). \tag{2.1}$$

The spin-unrestricted computational methods were applied to all the systems in the text. The test results of different methods on energy barriers are presented in electronic supplementary material, table S1. There is a little deviation between RI-B2KPLYP/ma-def2-TZVP and CCSD(T)/CBS calculations. Considering the computational cost, the accuracy at the B3LYP/6-311++G** level is also acceptable. The B3LYP, RI-B2KPLYP and CCSD(T) methods were realized by the Gaussian 09 [46] and ORCA 3.0 [47] program packages. The polarized continuum model [48] of integral equation form [49,50] (IEF) was used to evaluate the solvent effects. For ionic pairs with unknown packing modes, their stabilities were presented by Born–Haber cycles. The lattice potential energies were empirically estimated by the ionic pair volumes inside a contour of 0.001 electrons Bohr^{-3} at the HF/6-311++G**// B3LYP/6-311++G** level. It must be noted that these calculations only involve the isolated states. For 1 : 1 salts, the specific equation on the lattice potential energies is presented as follows [51]:

$$U_{\mathrm{POT}} = 2\left(\frac{28.0}{\sqrt[3]{V}} + 12.4\right)\ \mathrm{kcal\ mol^{-1}}, \tag{2.2}$$

where V represents the ionic pair (formula unit) volume in nm^3. The lattice enthalpy corrections for monatomic, linear and polyatomic ions are −0.5RT, 0.5RT and RT, respectively.

2.2. Solid physics

The PBE [52,53] method (a density functional with generalized gradient approximation) combined with on the fly generation ultrasoft [54] potential for Materials Studio 8.0 [55] (OTFG_80) and semi-empirical dispersion correction of Tkatchenko & Scheffler [56] was used for periodic boundary condition. Brillouin zone sampling on a grid of spacing $2\pi \times 0.07\ \mathrm{Å}^{-1}$ and a plane-wave basis set cut-off of 630 eV were set. This calculation was realized by the CASTEP [57] plane-wave code.

2.3. Potential energy surfaces

There are three kinds of optimized geometries on the PESs, i.e. the local minimum energy points, the first-order saddle points and the minimum energy crossing points (MECPs). The local minimum energy points involve the equilibrium geometries of reactants, intermediates (IMs) and products which locate at

the lowest energy points within the $3N-6$ dimensional spaces of PESs (suppose a nonlinear molecule, N represents the atom number of molecule). The first-order saddle points involve the transition states (TSs) which locate at the minimum energy points except for only one direction (only valid for the selected cell of periodic boundary condition) of the $3N-6$ dimensions. The MECPs involve the crossings between the two spin states which locate at the minimum energy points within the $3N-7$ dimensional subspaces of PESs of the crossing hyperlines. They can be optimized along the first and second gradients of the square of the difference between the total energies of two states. The optimized *xyz* coordinates in this paper are presented in the electronic supplementary material. The dimensionality of PESs can be checked by the frequency or phonon calculations. All reactants, IMs, products and MECPs have no imaginary frequency, and TSs have only one imaginary frequency. The thermodynamic properties can also be deduced by frequency or phonon calculations. The activation free energy barriers were derived by the differences counted from TSs or MECPs to reactants or products. Unless otherwise specified, the barriers mainly stand for the activation free energy barriers at 298 K calculated at the B3LYP/6-311++G** level in the text.

3. Results and discussion

3.1. Reaction pathways for phenylpentazole

PPZ consists of a pentazolyl group bonded to a phenyl group. Beside PPZ (singlet state), PPZ-R (triplet state) and PPZ-RA (doublet state) have the same symmetry of C_{2v}. For the sake of argument of PESs on the changes of atomic positions, the labels of PPZ and their derivatives are shown in figure 1.

The reactions starting with a single molecule usually impart two kinds of modes, i.e. isomerization and dissociation. As to the same product, it can be achieved directly or indirectly. In this way, the PESs around PPZ and their derivatives are presented in figures 2–4. As shown in figure 2, there are concerted and stepwise mechanisms for dissociation of PPZ to azidobenzene with evolution of dinitrogen. The concerted pathway involving the breakages of N_α–N_β and N_γ–N_γ bonds has a barrier of 16.8 kcal mol^{-1}. The stepwise pathway involves an IM, 1-azido-2-phenyldiazene, with a N_5 chain. Because the free energy of TS of the first step is higher than that of the second step, the determinant barrier of 28.4 kcal mol^{-1} for dissociation only involves the breakage of N_α–N_β bond in the first step. The IM can also dissociate into benzenediazonium cation and azide anion, and the effective barrier counted from PPZ is 31.9 kcal mol^{-1}. There is only stepwise pathway for the formation of PPZ via reaction between benzenediazonium cation and azide anion, i.e. the reverse pathway for dissociation. The determinant IM, azidophenyldiazene, is located in a shallow potential well for dissociating to azidobenzene and cyclizing to PPZ. The dissociation and cyclization barriers are 2.4 and 4.4 kcal mol^{-1}, respectively. The computational results are consistent with the previous study on the dissociation and formation of PPZ analogue [58,59].

The carbon–carbon coupling and proton transfer can produce isomers of PPZ. The coupling barriers for C_β–$C_{\beta'}$, C_γ–$C_{\gamma'}$, C_α–C_γ, C_β–C_δ, C_β–$C_{\gamma'}$ and C_α–C_δ are 99.1, 105.8, 109.4, 103.8, 105.7 and 104.1 kcal mol^{-1}, respectively. The proton transfers from C_β to C_α, from C_β to C_γ and from C_γ to C_β have the barriers of 94.7, 88.8 and 91.1 kcal mol^{-1}, respectively. These coupling and transfer reactions are endothermic. The processes impart above 75% contributions to barriers. Owing to the ultra-high barriers, they are difficult to initiate subsequent reactions at ambient condition.

The cleavages of C_α–N_α bonds can proceed along two different pathways. One involves the breakage of C_α–N_α and the coupling of C_α–N_β with a barrier of 62.8 kcal mol^{-1}, but the production is still PPZ. The other involves the breakage of C_α–N_α and the coupling of C_β–N_β with a barrier of 111.6 kcal mol^{-1}. The proton transfer from C_β to C_α can also form the same isomer with a barrier of 94.7 kcal mol^{-1}. At the thermodynamic point of view, the formation of benzenium cation and pentazolate anion is endothermic associated with a free energy of 176.6 kcal mol^{-1}. The preferred pathway for PPZ is dinitrogen evolution at ambient condition. The barriers for C–C coupling and proton transfer are lower than 176.6 kcal mol^{-1}. Thus, they are possible at high-energy condition.

3.2. Reaction pathways for phenylpentazole radical

As shown in figure 3, PPZ-R lies 69.7 kcal mol^{-1} (adiabatic excited energy) above PPZ. There are several entrances to the singlet states, such as carbon–carbon coupling, proton transfer and non-planarization. Each pathway for carbon–carbon coupling undergoes a triplet TS, a triplet IM and a MECP. The effective barriers, counted from PPZ to TS (or MECP) which has the highest potential energies along the pathway, for C_α–C_γ and C_β–C_δ couplings are 42.4 and 35.0 kcal mol^{-1}, respectively. The proton transfer from C_β

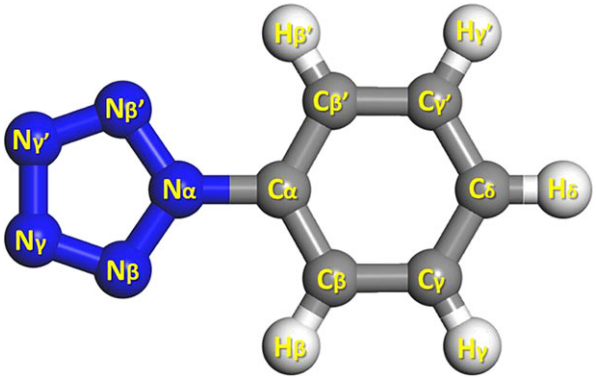

Figure 1. Atomic labels for PPZ, PPZ-R and PPZ-RA and their derivatives.

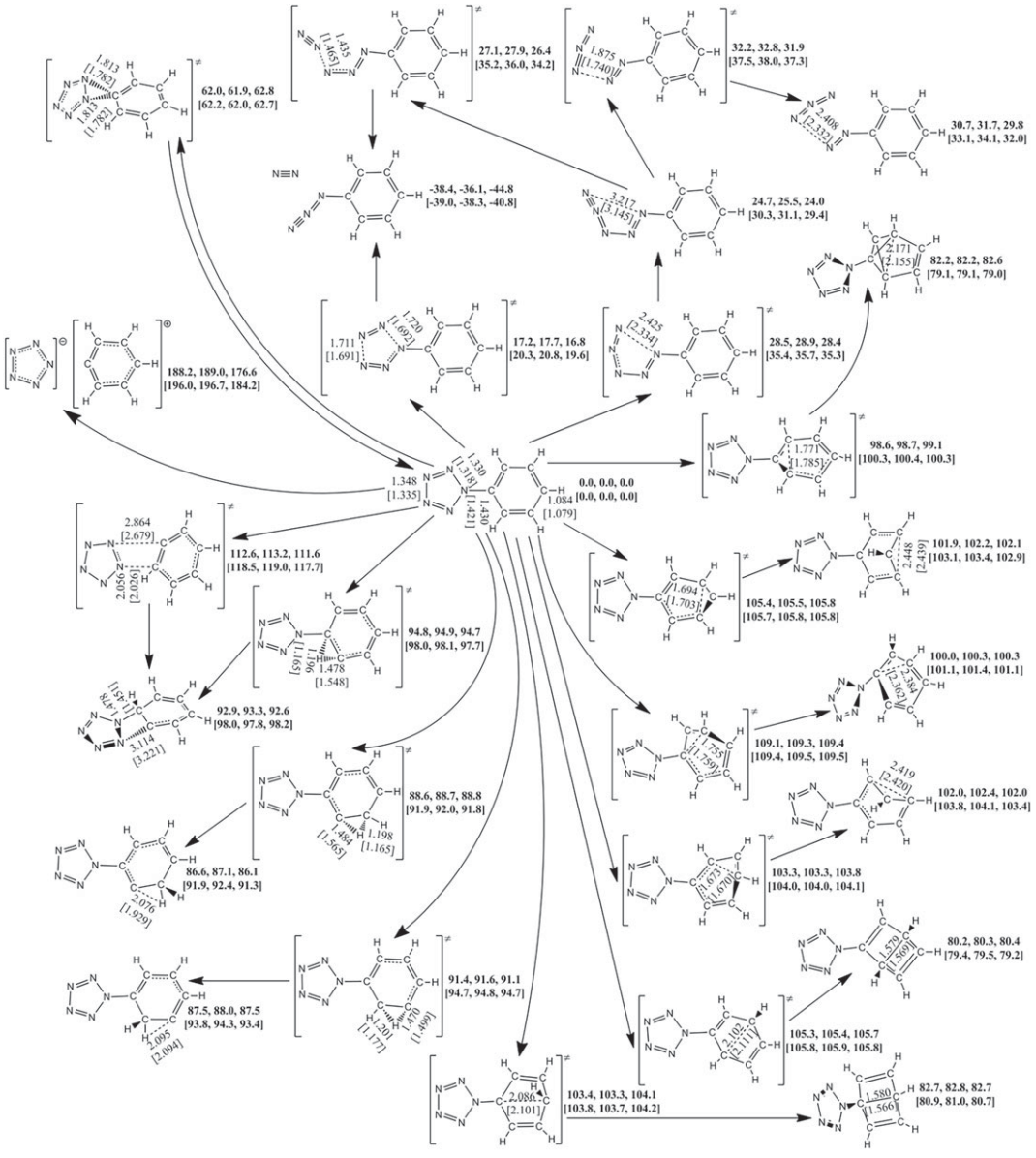

Figure 2. The PES scanning result for PPZ calculated at the B3LYP/6-311++G** and RI-B2KPLYP/ma-def2-TZVP (in brackets) levels. The energy (sum of total electronic energy and ZPC at front, enthalpy of 298 K at middle and free energy of 298 K at back) scales are offset to 0 kcal mol^{-1} for PPZ as the reference. The crucial bond lengths are labelled in Å.

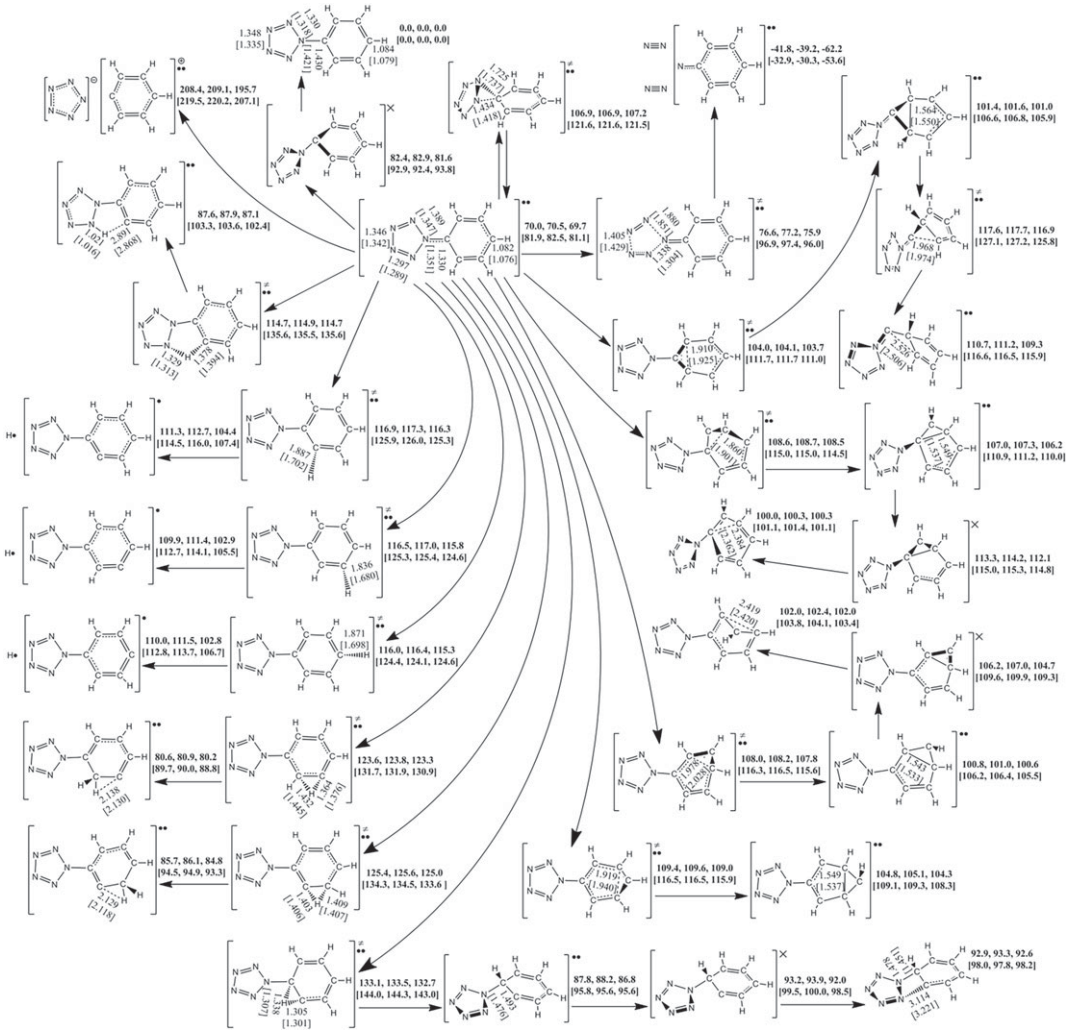

Figure 3. The PES scanning result for PPZ-R calculated at the B3LYP/6-311++G** and RI-B2KPLYP/ma-def2-TZVP (in brackets) levels. The energy (sum of total electronic energy and ZPC at front, enthalpy of 298 K at middle and free energy of 298 K at back) scales are offset to 0 kcal mol^{-1} for PPZ as the reference. The crucial bond lengths are labelled in Å.

to C_α can also lead to the singlet state. The determinant pathway is the isomerization in the triplet system with a barrier of 63.0 kcal mol^{-1}. The direct pathway from PPZ-R to PPZ undergoes a non-planarized MECP with a barrier of 11.9 kcal mol^{-1}.

The C_β–$C_{\beta'}$ coupling has a barrier of 34.0 kcal mol^{-1} which is lower than that of C_γ–$C_{\gamma'}$ coupling by 5.3 kcal mol^{-1}, and the further reaction can produce a structure with a carbon atom bridging a cyclopentyl group and a pentazolyl group. The free energy of the bridging structure is higher than that of the C_β–$C_{\beta'}$ coupling structure by 8.3 kcal mol^{-1}.

The proton transfer from C_β to N_β has a barrier of 45.0 kcal mol^{-1}, and the endothermic process is associated with a free energy of 17.4 kcal mol^{-1}, but it cannot form pentazole successively. The proton transfers from C_β to C_γ and from C_γ to C_β have the barriers of 53.6 and 55.3 kcal mol^{-1}, respectively. The deprotonations of H_α, H_γ and H_δ have the barriers of 46.6, 46.1 and 45.6 kcal mol^{-1}, respectively. They are endothermic, and impart about 28% contributions to barriers.

The cleavage of C_α–N_α accompanied by the coupling of C_α–N_β gives rise to no chemical change for PPZ-R. At the thermodynamic point of view, the dissociation energy of the formation of benzenium radical cation and pentazolate anion is 126.0 kcal mol^{-1}. Although the barrier of dinitrogen evolution is only 6.6 kcal mol^{-1}, the C–C couplings, proton transfers and deprotonations still have the lower energies than 176.6 kcal mol^{-1} for C–N cleavage of PPZ. Thus, the possible pathway of the formation of PZA at high-energy condition is that PPZ is excited to PPZ-R at the first step, the proton is abstracted at the second step and PZA is formed at the subsequent step.

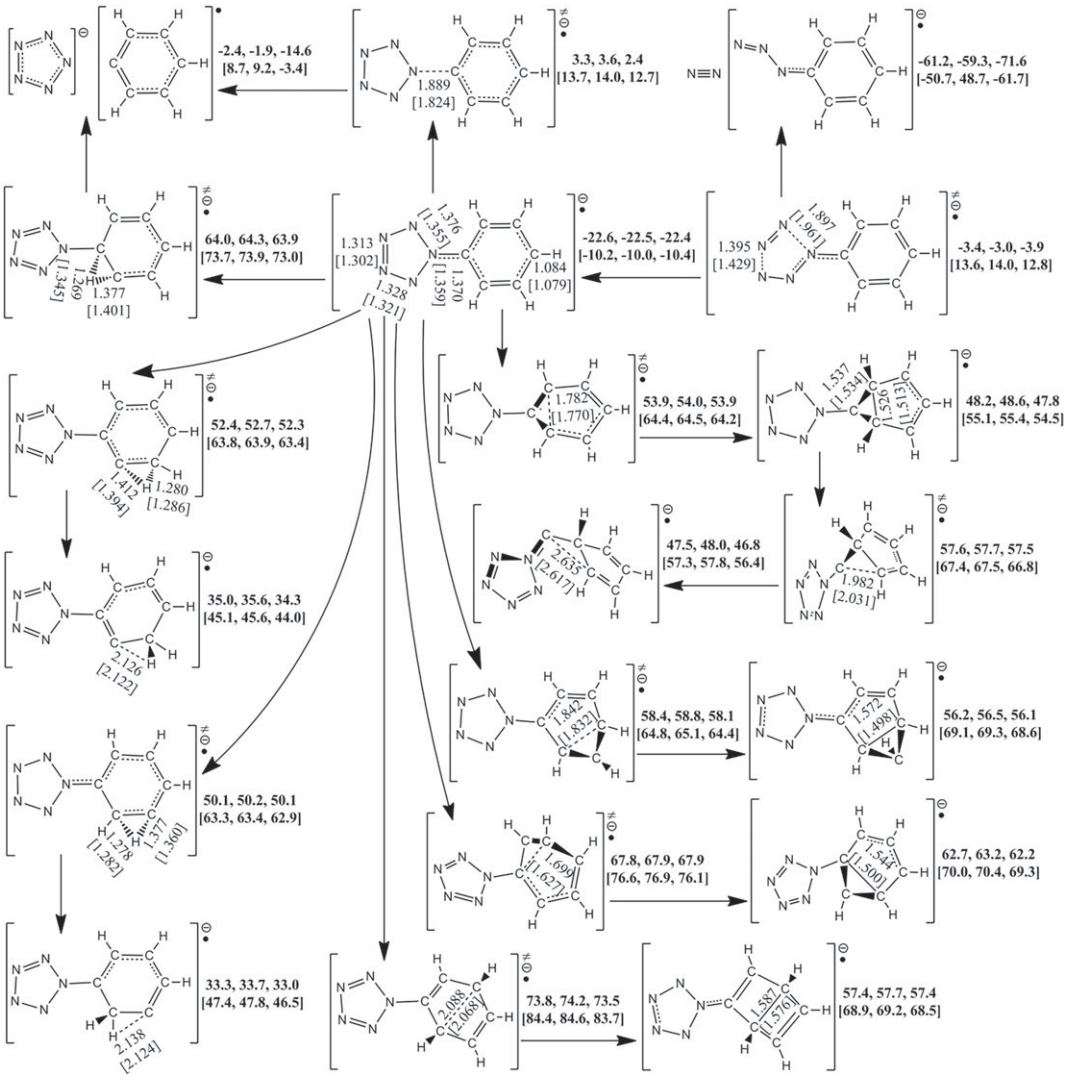

Figure 4. The PES scanning result for PPZ-RA calculated at the B3LYP/6-311++G** and RI-B2KPLYP/ma-def2-TZVP (in brackets) levels. The energy (sum of total electronic energy and ZPC at front, enthalpy of 298 K at middle and free energy of 298 K at back) scales are offset to 0 kcal mol^{-1} for PPZ as the reference. The crucial bond lengths are labelled in Å.

3.3. Reaction pathways for phenylpentazole radical anion

As shown in figure 4, the free energy of PPZ-RA is higher than that of PPZ by 22.4 kcal mol^{-1} (adiabatic ionization potential (IP) for PPZ-RA). Similar to PPZ and PPZ-R, the pathways of carbon–carbon coupling and proton transfer have the very high barriers, and need external heat. The coupling barriers for C_β–$C_{\beta'}$, C_β–C_δ, C_α–C_γ and C_β–$C_{\gamma'}$ are 76.3, 80.5, 90.3 and 95.9 kcal mol^{-1}, respectively. The C_β–$C_{\beta'}$ coupling product can isomerize to a structure with a carbon atom bridging two five-membered ring groups with an effective barrier counted from PPZ-RA of 79.9 kcal mol^{-1}. The proton transfers from C_β to C_γ and from C_γ to C_β have the barriers of 74.7 and 72.5 kcal mol^{-1}, respectively. The formation of pentazolate anion can proceed along two different pathways, and absorb 7.8 kcal mol^{-1} heat. One is the proton transfer from C_β to C_α leading to the cleavage of C_α–N_α bond with a barrier of 86.3 kcal mol^{-1}. The other is the direct cleavage of C_α–N_α bond which competes against the dinitrogen evolution. The barriers for the pentazolate anion formation and the dinitrogen evolution are 24.8 and 18.5 kcal mol^{-1} at the B3LYP/6-311++G** level, respectively. In contrast to the calculated result at the RI-B2KPLYP/ma-def2-TZVP level, the difference between the two barriers is smaller and the high–low relationship is still kept, i.e. 23.1 kcal mol^{-1} for the pentazolate anion formation and 23.2 kcal mol^{-1} for the dinitrogen evolution. The same trend was reported using the average of three high accuracy methods [11]. As shown in electronic supplementary material, table S2, the solvent effect of THF has little impact on the correlative barriers.

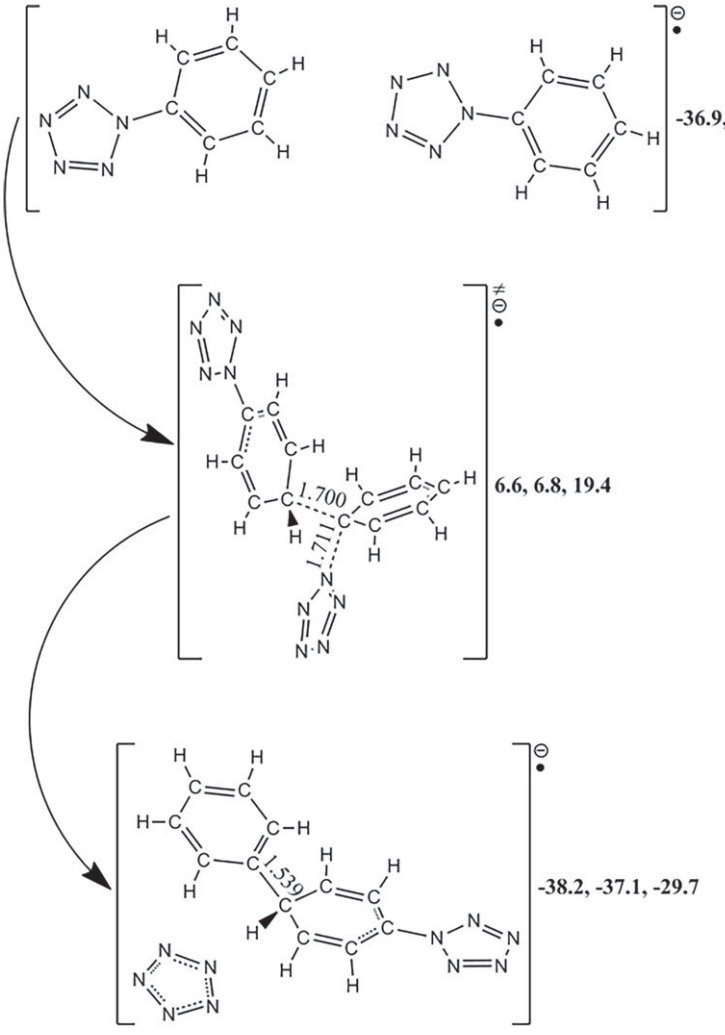

Figure 5. The PZA formation pathway starting with PPZ-RA and PPZ calculated at the B3LYP/6-311++G** level. The energy (sum of total electronic energy and ZPC at front, enthalpy of 298 K at middle and free energy of 298 K at back) scales are offset to 0 kcal mol^{-1} for two PPZs as the reference. The crucial bond lengths are labelled in Å.

It must be prudent to re-compute the two critical barriers using the theoretical method as accurately as possible. The re-calculated result survey that the high–low relationship between the two barriers at the CCSD(T)/CBS level is opposite to those at the B3LYP/6-311++G** and RI-B2KPLYP/ma-def2-TZVP levels, i.e. 25.5 kcal mol^{-1} for the pentazolate anion formation and 26.7 kcal mol^{-1} for the dinitrogen evolution at the CCSD(T)/CBS level.

The radical production is another important issue. As shown in figure 5, the reaction between PPZ and PP-RA can produce pentazolate anion and biphenyl pentazole with a barrier of 47.9 kcal mol^{-1}. Although the long-range interaction of the reaction complex causes the deeper potential well by 14.3 kcal mol^{-1}, the formation barrier of pentazolate anion in the presence of PPZ is higher than that in the absence of PPZ indeed. The possible pathway may be the formation of phenyl radical at the first step, and spontaneous formation of polyphenyl at the second step. It is the possible origin of gel [10].

3.4. Electron transfer in sodium phenylpentazole

Besides self-dissociation, the stability of PPZ-RA also depends on the electron transfer from it to sodium cation. The process generally undergoes the formation of the neutral counterparts of ions without a barrier. If the electron transfer free energy has a negative value, the determinant factor on stability will be the dissociation barrier of PPZ. Otherwise, the positive energy will provide an extra barrier to PPZ. The Born–Haber cycle shown in figure 6 indicates that the IP value of PPZ-RA is not large

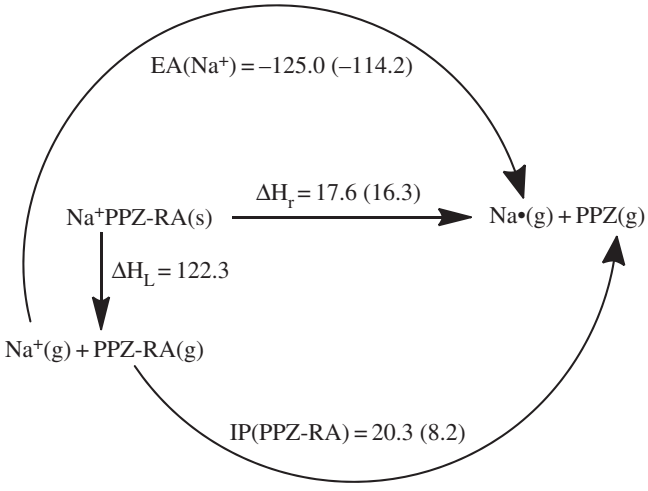

Figure 6. Born–Haber cycle in kcal mol^{-1} for the dissociative reaction of solid Na^+PPZ-RA. The IP and EA are calculated at the B3LYP/6-311++G** and the CCSD(T)/CBS (in parentheses) levels, and the lattice enthalpy is estimated by an ionic pair volume of 0.192 nm^3.

enough to cover the electron affinity (EA) value of sodium cation, but when the lattice enthalpy is taken into account, the electron transfer enthalpy (17.6 kcal mol^{-1} at 298 K) becomes positive. The reactivity depends on the free energy change. Consequently, the contribution of entropy cannot be neglected. These kinds of reactions always go through the entropy increasing process which can reduce the enthalpy. The dinitrogen evolution barrier for PPZ is lower than the PZA formation barrier from PPZ-RA by 8.0 kcal mol^{-1} at 298 K. Thus, the entropy correction ($T\Delta S$) at 298 K must be less than 9.6 kcal mol^{-1} for the dominant formation of pentazolate anion. Given the calculated entropies of PPZ and Na radical of 90.7 and 36.7 cal mol^{-1} K^{-1}, respectively, the entropy of sodium PPZ of more than 94.6 cal mol^{-1} K^{-1} can meet the requirement. Some known sodium salts can be used as references, e.g. the entropies of sodium azide, sodium cyanide, sodium cyanate, sodium nitrate, sodium formate, sodium hydrogen carbonate and sodium acetate of 23.2, 16.8, 20.7, 22.2, 19.8, 20.9 and 19.1 cal mol^{-1} K^{-1}, respectively [60]. As such, the goal of 94.6 cal mol^{-1} K^{-1} is hard to achieve. If the entropy of sodium azide is used to estimate the electron transfer reaction free energy at 298 K, it is equal to −13.5 kcal mol^{-1}. The lattice energy for the crystalline state almost represents the limitation of binding ability. The ionic pair can be formed at a very low temperature. In consideration of the barrier of radical anion mechanism of 25.5 kcal mol^{-1} at the CCSD(T)/CBS level, the pentazolate anion formation should be handled at a relative high temperature which can also lead to the dissociation of PZA. The computational result is consistent with the experimental evidence which indicated that PPZ treated with clean Na leads to dissociation, but PZA can be formed by PPZ treated with passivated Na [12].

3.5. Reaction pathways for phenylpentazole and *m*-chloroperbenzoic acid

Owing to the multiple reactive sites for multi-molecule, the oxidation mechanisms of *m*-CPBA are more complex. Figures 7–9 present the information on the reactions of PPZ, PZPolA and PZPol with *m*-CPBA as much as possible. There are two isomers of *m*-CPBA, i.e. the chorophenyl points either to the same direction as the carbonyl or to the opposite direction. The two isomers have almost the same potential energy with a conversion barrier of 5.9 kcal mol^{-1}. The detailed pathways for *m*-CPBA are presented in electronic supplementary material, figure S1. Thus, the computational result will not be affected by the selection of isomers.

The reactions between PPZ and *m*-CPBA can proceed along two kinds of pathways, i.e. the oxidizations of pentazolyl and phenyl groups. The transition states on *m*-CPBA concern the breakages of peroxyl bond and the transfers of proton. As shown in figure 7, the barriers of the proton transfers to the original carbonyl groups are usually higher than those of the proton transfers to the original peroxyl groups. Thus, the latter oxidations were not involved in further consideration.

The cleavage of C_α–N_α is not induced by the attack of the oxygen of *m*-CPBA on the C_α of PPZ, but it forms a benzene oxide structure with a barrier of 35.5 kcal mol^{-1}. The oxidizations of N_α, N_β and N_γ of PPZ have the barriers of 53.5, 36.3 and 31.2 kcal mol^{-1}, respectively, and they involve the dinitrogen evolution, the N_β-oxo-PPZ formation and the N_γ-oxo-PPZ formation, respectively. The

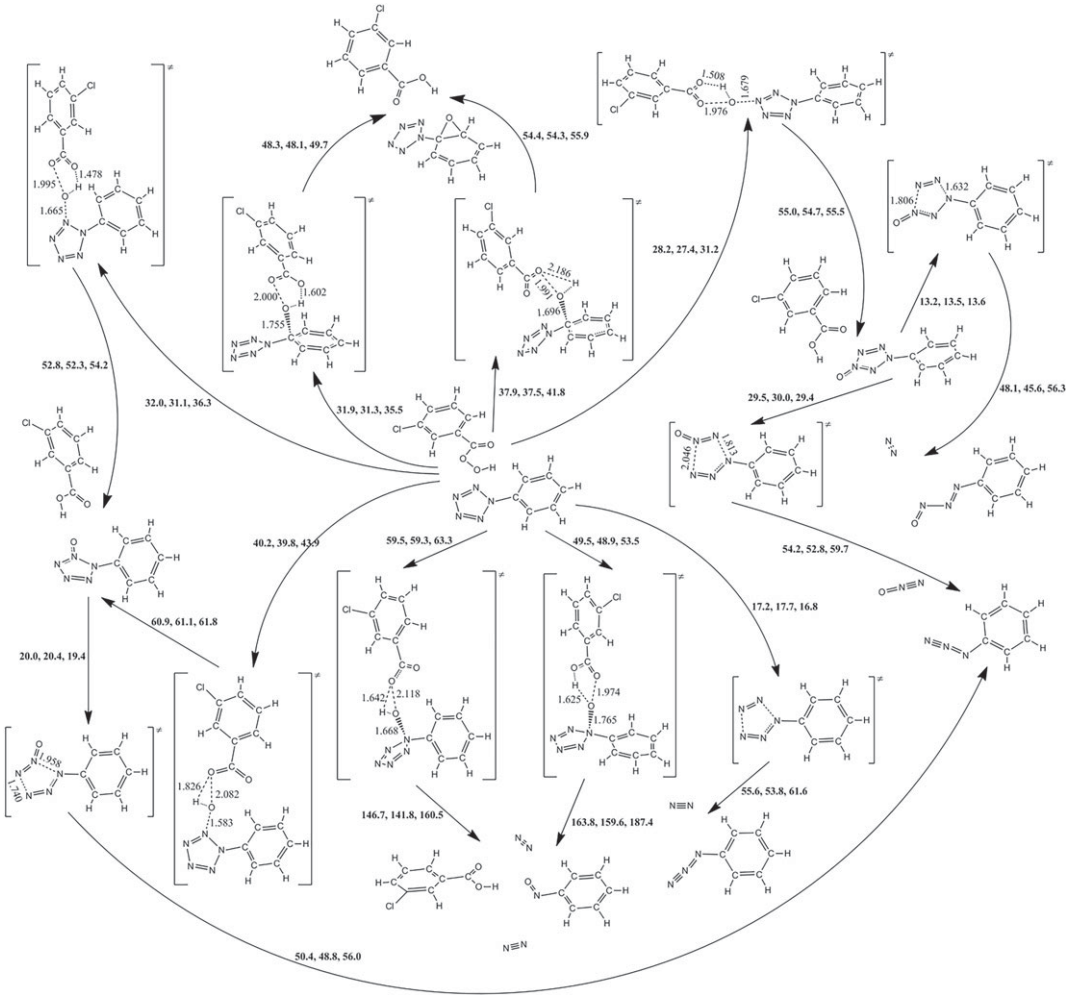

Figure 7. The PES scanning result for PPZ and *m*-CPBA calculated at the B3LYP/6-311++G** level. The activation energy barriers (sum of total electronic energy and ZPC at front, enthalpy of 298 K at middle and free energy of 298 K at back) are in kcal mol^{-1}. The crucial bond lengths are labelled in Å.

N_β-oxo-PPZ dissociates to azidobenzene with a barrier of 19.4 kcal mol^{-1}. The N_γ-oxo-PPZ dissociates to azidobenzene and nitrosophenyldiazene with the barriers of 29.4 and 13.6 kcal mol^{-1}, respectively.

According to the potential energy scanning result, the barriers of the reactions between PPZ and *m*-CPBA are higher than that of PPZ self-dissociation, and there is no pathway concerning the formation of PZA.

3.6. Reaction pathways for pentazolylphenolate anion and *m*-chloroperbenzoic acid

As shown in figure 8, the cleavage of C_α–N_α bond of PZPolA undergoes a MECP, and forms phenyl radical and PZA. It has a very high barrier of 60.2 kcal mol^{-1} which agrees with the previous computational investigation [8]. Comparatively, the dinitrogen evolution barrier of PZPolA is only 19.5 kcal mol^{-1}. Although it is one of the most kinetic stable PPZ derivatives [61].

The pentazolyl oxidization barriers in the PZPolA and *m*-CPBA system are approximate to those in the PPZ and *m*-CPBA system. The oxidizations of N_β and N_γ of PZPolA have the barriers of 35.2 and 32.5 kcal mol^{-1}, respectively. The oxidation of the C_α of PZPolA prefers to form benzoquinone and transfer the electron to pentazole. The barrier of 23.0 kcal mol^{-1} for formation of PZA means that it should compete against the dissociation.

3.7. Reaction pathways for pentazolylphenol and *m*-chloroperbenzoic acid

As shown in figure 9, the pentazolyl oxidizations in PZPol and *m*-CPBA systems are similar to PPZ and *m*-CPBA. The oxidizations of N_α, N_β and N_γ of PZPol have the barriers of 56.5, 38.6 and 33.9 kcal mol^{-1},

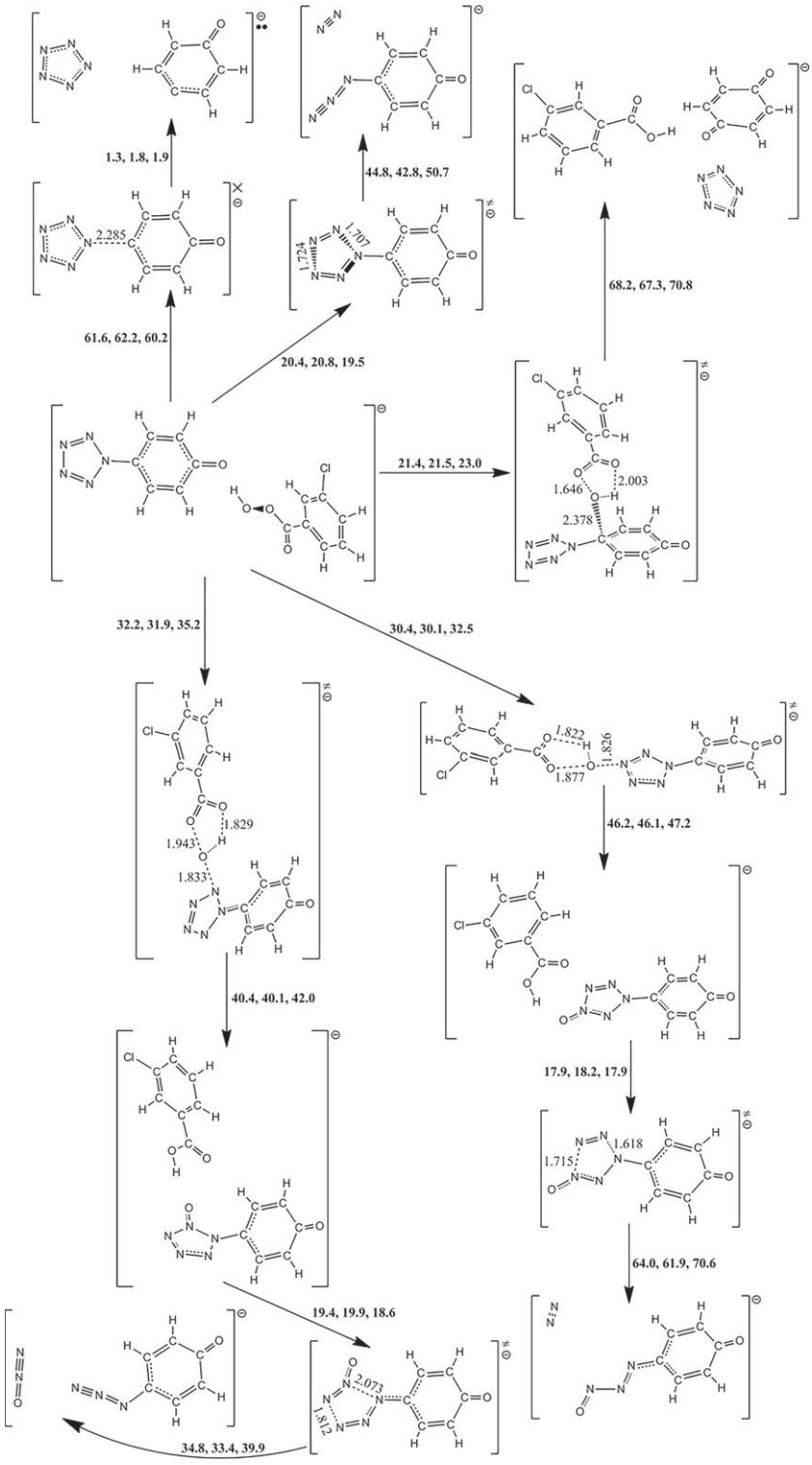

Figure 8. The PES scanning result for PZPolA and *m*-CPBA calculated at the B3LYP/6-311++G** level. The activation energy barriers (sum of total electronic energy and ZPC at front, enthalpy of 298 K at middle and free energy of 298 K at back) are in kcal mol^{-1}. The crucial bond lengths are labelled in Å.

respectively. The dissociation abilities of oxide products for PZPol and *m*-CPBA are the same as those for PPZ and *m*-CPBA. These reactions are not easy to realize.

The experimental attempt used phenol substance as the starting material [19]. The formation of quinone via the hydroxyl group deprotonation is the possible way to the goal of formation of PZA. The first strategy is the oxygen of *m*-CPBA attacking the C_α of PZPol, and then deprotonation. The

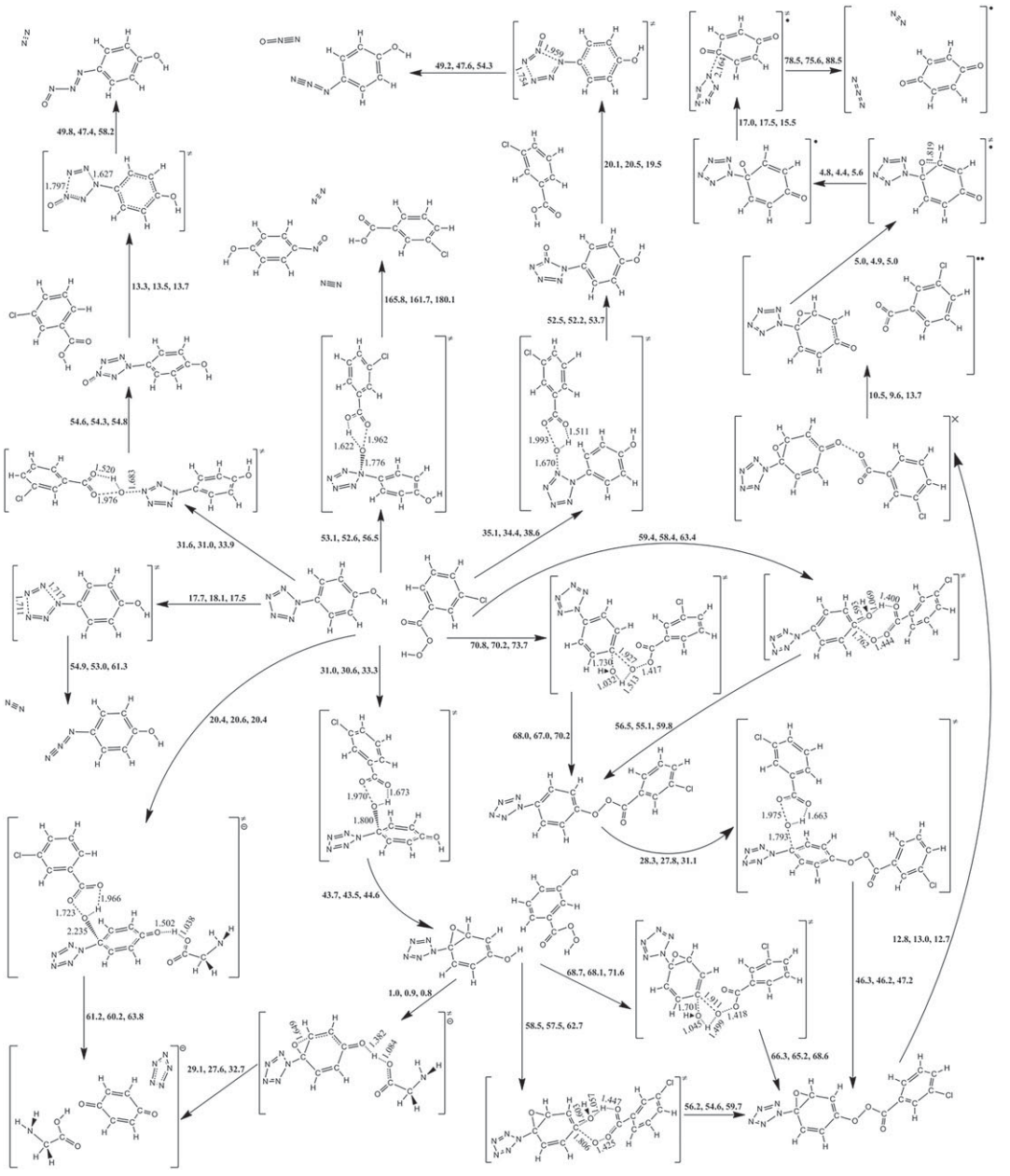

Figure 9. The PES scanning result for PZPol and *m*-CPBA calculated at the B3LYP/6-311++G** level. The activation energy barriers (sum of total electronic energy and ZPC at front, enthalpy of 298 K at middle and free energy of 298 K at back) are in kcal mol^{-1}. The crucial bond lengths are labelled in Å.

C_α oxidation involves the production of a phenol oxide structure with a barrier of 33.3 kcal mol^{-1}. The deprotonations of PZPol oxide can proceed along two different pathways: (1) a stepwise pathway to benzoquinone, dinitrogen and N_3 radical undergoes the dehydration with *m*-CPBA, the cleavage of peroxyl bond via a MECP, the cleavage of C_α–N_α bond, etc., with an effective barrier of 62.7 kcal mol^{-1} counted to the seven-membered ring TS of dehydration; (2) the glycinate anion absorbs the proton of PZPol oxide and the cleavage of C_α–N_α bond produce benzoquinone and PZA with a barrier of 0.8 kcal mol^{-1}. Mulliken analyses indicate that the electrons transfer to C_α in both TSs which makes the C_α–N_α bond weak, figure 10. The anionic systems provide the environments for the electrons transferring to pentazole fragments, just as the radical anion mechanism. According to the TS geometries on the active sites, the dehydrations are divided into two mechanisms, i.e. four-membered and seven-membered rings, and the dehydration barrier of the former mechanism is higher than that of the latter mechanism. The second strategy is dehydration in advance, and then C_α oxidation, cleavage of peroxyl bond, the cleavage of C_α–N_α bond, etc. The terminal productions are the same as the first strategy.

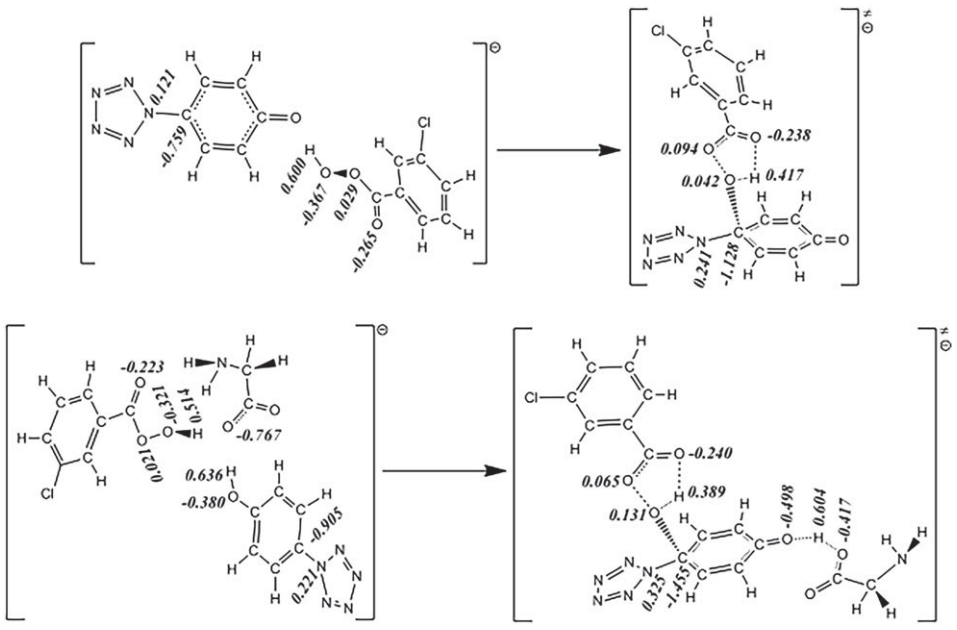

Figure 10. Mulliken charges of active atoms for formations of PZA from reactants to TSs.

Table 1. The crucial activation energy barriers for formations of PZA and dissociations of arylpentazoles in kcal mol^{-1} excluding ZPCs with and without the solvent effects.

	$\Delta E^{\neq}$(B3LYP[a])				$\Delta E^{\neq}$(RI-B2KPLYP[b])
transition states	gas	water	methanol	acetonitrile	gas
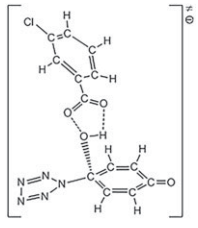	22.2	19.6	19.7	19.6	25.3
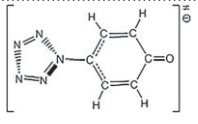	23.1	23.0	23.0	23.0	26.3
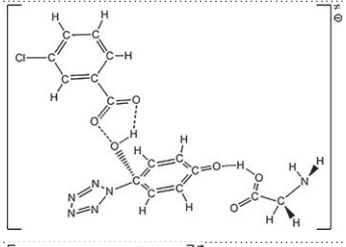	22.3	22.0	22.0	22.0	27.4
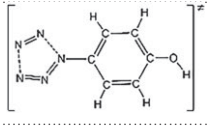	20.2	22.0	21.9	22.0	23.4

[a]Using the 6-311++G** basis set.
[b]At the RI-B2KPLYP/ma-def2-TZVP//B3LYP/6-311++G** level.

The determinant step is also the seven-membered ring dehydration with a barrier of 63.4 kcal mol^{-1}. The third strategy is the concerted mechanism, i.e. the deprotonation is simultaneous with the cleavage of C_α–N_α bond. The tri-molecular reaction among PZPol, *m*-CPBA and glycinate anion produces

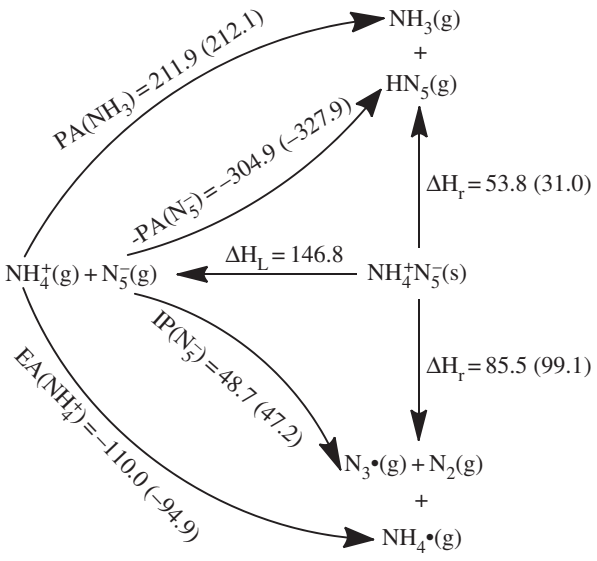

Figure 11. Born–Haber cycles in kcal mol^{-1} for the dissociative reaction of solid $NH_4^+N_5^-$. The IP, EA and PA are calculated at the B3LYP/6-311++G** and the CCSD(T)/CBS (in parentheses) levels, and the lattice enthalpy is estimated by an ionic pair volume of 0.104 nm^3.

benzoquinone, glycine and PZA with a barrier of 20.4 kcal mol^{-1} which is higher than the barrier of dinitrogen evolution of 17.5 kcal mol^{-1}. Based on the solvent effects shown in table 1, the reaction barriers of PZPolA and *m*-CPBA are decreased by 2.6 kcal mol^{-1} for water, 2.5 kcal mol^{-1} for methanol and 2.6 kcal mol^{-1} for acetonitrile. There are no significant impacts on the competitive reactions. Thus, PZPolA is more feasible than PZPol on PZA formation.

3.8. Electron and proton transfers in $(N_5)_6(H_3O)_3(NH_4)_4Cl$

Primarily the stability of $(N_5)_6(H_3O)_3(NH_4)_4Cl$ is simplified as the dissociations of two ionic pairs, i.e. $NH_4^+N_5^-$ and $H_3O^+N_5^-$. The complete contact between H_3O^+ and N_5^- partly supports the reasonability for the assumption. Because the *cyclo*-N_5 radical (removal of one electron of PZA) does not locate at the local minimum point of PES, the dissociation products of N_3 radical and N_2 are used for the adiabatic IP calculation. The Born–Haber cycles on $NH_4^+N_5^-$ shown in figure 11 indicate the reaction enthalpy of electron transfer of 85.5 kcal mol^{-1} is higher than that of proton transfer of 53.8 kcal mol^{-1}, i.e. the proton transfer is dominant. These enthalpies need to be corrected by the entropies. The calculated entropies of NH_3 and HN_5 are 46.0 and 63.8 cal mol^{-1} K^{-1}, respectively, and the referenced solid entropies of ammonium azide, ammonium nitrate and ammonium hydrogen carbonate are 26.9, 36.1 and 28.9 cal mol^{-1} K^{-1} [60], respectively. If the entropy of ammonium azide is used to estimate the proton transfer reaction free energy of $NH_4^+N_5^-$ at 298 K, it is equal to 29.1 kcal mol^{-1}. It is thermodynamically stable enough to prevent the proton transfer. Thus, the stability of solid $NH_4^+N_5^-$ is decided by the dissociation barrier of PZA.

The Born–Haber cycles on $H_3O^+N_5^-$ shown in figure 12 indicate that the proton transfer is more dominant than the electron transfer thermodynamically. Although the proton transfer enthalpy of 15.1 kcal mol^{-1} at the B3LYP/6-311++G** level is sufficient to overcome the entropy correction, a more accurate value of 1.1 kcal mol^{-1} at the CCSD(T)/CBS level cannot assure an extra barrier for the enhancement of stability of HN_5. However, in the absence of the entropies of hydronium salts, the calculation of $(N_5)_6(H_3O)_3(NH_4)_4Cl$ in the crystalline state was put forward. Except for the removal of three hydrogen atoms conjugated to each oxygen atom, the initial crystal structure from calculation was analogous to that from experiment [19]. The geometry optimization task was performed without the symmetry constrain and with the constant cell. Then the phonon calculation result deduced the thermodynamic properties. The entropy per $(N_5)_{6/7}(H_3O)_{3/7}(NH_4)_{4/7}Cl_{1/7}$ at 298 K of 33.6 cal mol^{-1} K^{-1} approximately represents that of $H_3O^+N_5^-$. Combined with the calculated entropies of H_2O and HN_5 of 45.1 and 63.8 cal mol^{-1} K^{-1}, respectively, the proton transfer reaction free energies of $H_3O^+N_5^-$ are −7.3 and −21.3 kcal mol^{-1}, if the reaction enthalpies are calculated at the B3LYP/6-311++G** and

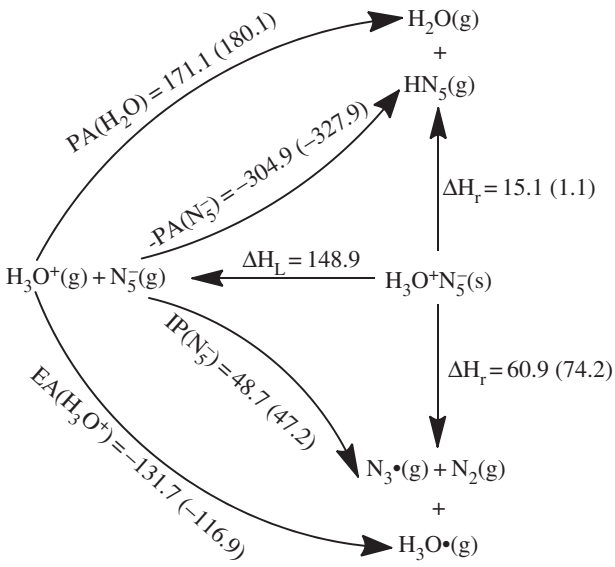

Figure 12. Born–Haber cycles in kcal mol^{-1} for the dissociative reaction of solid $H_3O^+N_5^-$. The IP, EA and PA are calculated at the B3LYP/6-311++G** and the CCSD(T)/CBS (in parentheses) levels, and the lattice enthalpy is estimated by an ionic pair volume of 0.110 nm^3.

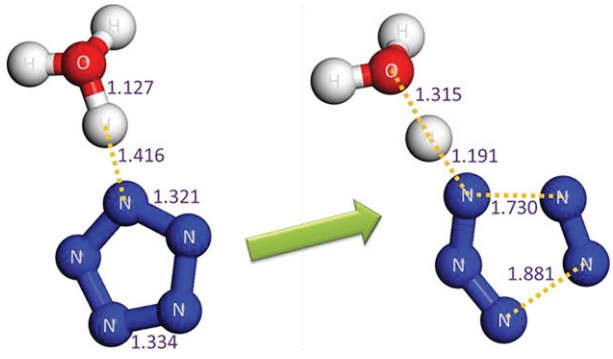

Figure 13. The crucial fragments of the optimized crystalline state of $(N_5)_6(H_3O)_3(NH_4)_4Cl$ for the dissociation from reactant to TS. The distances calculated at the PBE/OTFG_80 level are labelled in Å. The activation energy barrier including ZPC, activation enthalpy barrier at 298 K and activation free energy barrier at 298 K calculated at the PBE/OTFG_80 level are 25.9, 27.5 and 24.7 kcal mol^{-1}, respectively. The cell parameters and atomic positions of TS are presented in the electronic supplementary material.

the CCSD(T)/CBS levels, respectively. It surveys that the proton transfer in $H_3O^+N_5^-$ produces H_2O and HN_5 spontaneously. The subsequent reaction for HN_5 dissociation has the barriers of 19.1 and 21.2 kcal mol^{-1} at the B3LYP/6-311++G** and the CCSD(T)/CBS levels, respectively.

The concerted effect for the proton transfer and dinitrogen evolution in the solid $(N_5)_6(H_3O)_3(NH_4)_4Cl$ is shown in figure 13. The closest non-bond H–N distance in the equilibrium structure is only 1.416 Å. It tends to form H–N covalence bond together with the breakage of PZA, and the dissociation process releases 7.4 kcal mol^{-1} heat. The dissociation barrier calculated at the PBE/OTFG_80 level is 24.7 kcal mol^{-1}. To test the reliability of the computational method, a comparative study on the dinitrogen evolution barriers of PPZ excluding ZPCs indicates that the PBE/OTFG_80 method with a barrier of 17.2 kcal mol^{-1} underestimates the barriers by 2.6 and 4.9 kcal mol^{-1} at the B3LYP/6-311++G** and the CCSD(T)/CBS levels, respectively. When the thermal correction to Gibbs free energy at the B3LYP/6-311++G** level is used for the dissociation barrier of PPZ, it is down to 14.2 kcal mol^{-1}. Thus, the kinetic stability of the solid $(N_5)_6(H_3O)_3(NH_4)_4Cl$ is better than that of the isolated PPZ.

3.9. Stability of $M(N_5)_2(H_2O)_4$ (M = Co, Fe and Mn)

According to the structure of $M(N_5)_2(H_2O)_4{\cdot}4H_2O$ in the crystalline state [20,23], each metal atom coordinately bonds two pentazolyl groups and four water molecules, and there exists the long-range

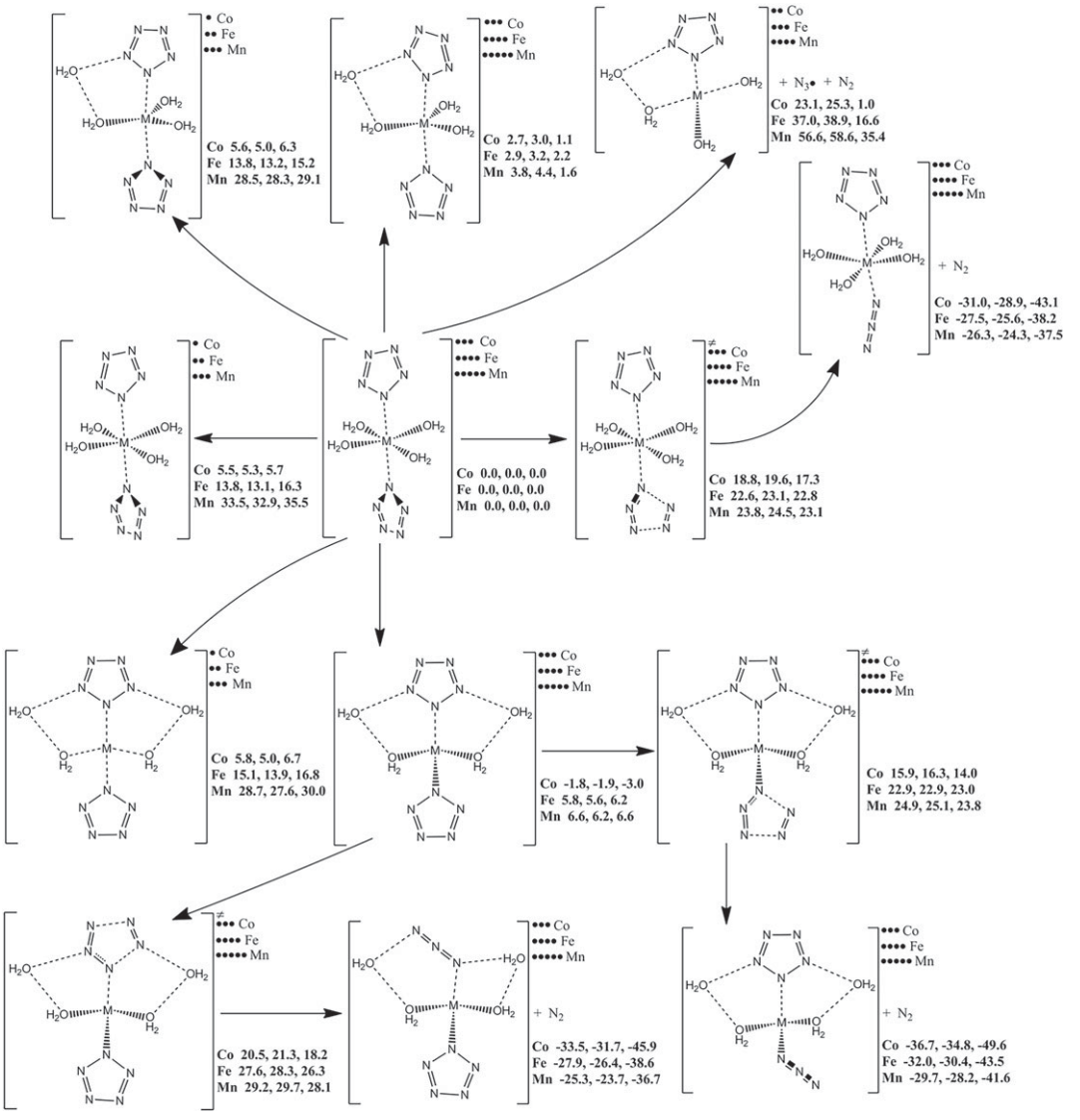

Figure 14. The PES scanning result for $M(N_5)_2(H_2O)_4$ (M = Co, Fe and Mn) calculated at the B3LYP/6-311++G**(HNO) + LanL2DZ(CoFeMn) level. The energy (sum of total electronic energy and ZPC at front, enthalpy of 298 K at middle and free energy of 298 K at back) scales are offset to 0 kcal mol^{-1} for $M(N_5)_2(H_2O)_4$ as the reference. The crucial bond lengths are labelled in Å.

interaction between the four crystal water molecules in the primitive cell and the coordination compound. Therefore, the stability of isolated state $Mn(N_5)_2(H_2O)_4$ can stand for that of crystalline state in a great part. The spin state and coordination must be revealed in the first place. The potential energy scanning result is shown in figure 14. The quartet $Co(N_5)_2(H_2O)_4$ imparts the quasi-octahedral structure. Across a Co atom, the two pentazolyl groups are perpendicular to each other. As to the doublet states, the four-coordinated $Co(N_5)_2(H_2O)_2{\cdot}2H_2O$ and the five-coordinated $Co(N_5)_2(H_2O)_2{\cdot}H_2O$ have the same potential energy level as six-coordinated $Co(N_5)_2(H_2O)_4$ which lies 5.7 kcal mol^{-1} above its quartet state. It demonstrates that the pentazolyl group is a weak ligand for Co, and the coordination compound imparts the high-spin state. The prediction can be verified by the measurement of magnetic moment. As to the quartet states, the potential energy of the six-coordinated $Co(N_5)_2(H_2O)_4$ is lower than that of the five-coordinated $Co(N_5)_2(H_2O)_2{\cdot}H_2O$ by 1.1 kcal mol^{-1}, but higher than that of the four-coordinated $Co(N_5)_2(H_2O)_2{\cdot}2H_2O$ by 3.0 kcal mol^{-1}. It demonstrates that the binding ability of the coordinate bond of water molecule is inferior to that of the crystal waters at the double sides of the pentazolyl group which is consistent with the space occupancy of the crystal waters in crystalline state. The electron transfer in $Co(N_5)_2(H_2O)_4$ produces triplet $Co(N_5)(H_2O)_3{\cdot}H_2O$, N_3 radical and N_2 with a free energy change of 1.0 kcal mol^{-1} at 298 K. The slight positive energy is difficult to prevent the

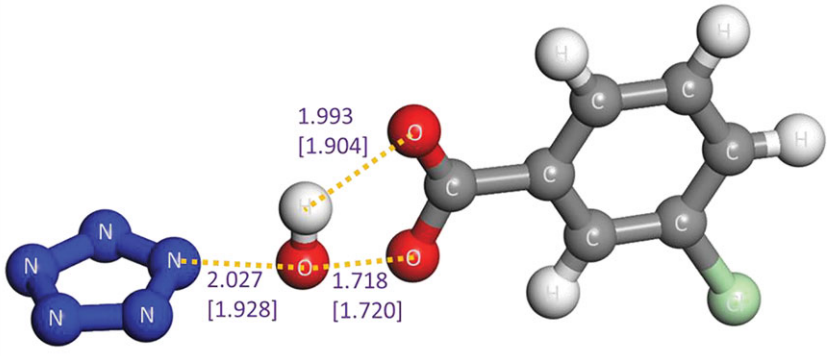

Figure 15. The optimized TS of reaction between PZA and *m*-CPBA. The system possesses one negative charge. The distances calculated at the B3LYP/6-311++G** and RI-B2KPLYP/ma-def2-TZVP (in parenthesis) levels are labelled in Å. The activation energy barrier including ZPC, activation enthalpy barrier at 298 K and activation free energy barrier at 298 K calculated from complex of PZA and *m*-CPBA to TS are 17.1, 16.9 and 19.0 kcal mol^{-1} at the B3LYP/6-311++G** level, respectively, and 22.6, 23.3 and 21.5 kcal mol^{-1} at the RI-B2KPLYP/ma-def2-TZVP level, respectively.

subsequent reaction. The dinitrogen evolution of $Co(N_5)_2(H_2O)_4$ has a barrier of 17.3 kcal mol^{-1} which is at the same level of PPZ. The dissociation of the exposed pentazolyl group in $Co(N_5)_2(H_2O)_2{\cdot}2H_2O$ has a barrier of 14.0 kcal mol^{-1}. But the dissociation of the pentazolyl group confined by the crystal waters has a higher barrier of 18.2 kcal mol^{-1}. Thus, the confinement effect of the crystal waters is beneficial to the kinetic stability of $Co(N_5)_2(H_2O)_4{\cdot}4H_2O$ in the crystalline state. The most stable Fe and Mn coordination compounds are quintet $Fe(N_5)_2(H_2O)_4$ and sextet $Mn(N_5)_2(H_2O)_4$. Their dissociation barriers are 22.8 and 23.1 kcal mol^{-1}, respectively. The dissociation barriers of the pentazolyl groups confined by the crystal waters for quintet $Fe(N_5)_2(H_2O)_2{\cdot}2H_2O$ and sextet $Mn(N_5)_2(H_2O)_2{\cdot}2H_2O$ are 26.3 and 28.1 kcal mol^{-1}, respectively. Consequently, Fe and Mn coordination compounds are more stable than Co coordination compound.

3.10. Stability of isolated pentazolate anion

The stability of a substance generally hinges on the two aspects, i.e. the decomposability of itself and the reactivity with other substances in the system. Without a doubt, PZA has a sufficient energy barrier without ZPC of above 25 kcal mol^{-1} for the dinitrogen evolution according to our (26.3, 28.6 and 28.7 kcal mol^{-1} at the B3LYP/6-311++G**, the RI-B2KPLYP/ma-def2-TZVP and the CCSD(T)/CBS levels, respectively) and other calculations [4–6]. As to the reactivity of PZA, a similar TS as the reaction between oxo-PPZ and *m*-CPBA is found. As shown in figure 15, the TS involves the breakage of peroxyl bond, proton transfer to original carbonyl group and oxygen atom approach to pentazolyl group that indicates the formation of oxo-PZA. The pathway has a low barrier of 19.0 kcal mol^{-1}. Based on the PES scan around oxo-PZA, the optimum dissociation pathway involves the production of N_3O^- and N_2 in the first step, and the production of triplet NO^- in the second step. The re-calculation of published result [62] at the B3LYP/6-311++G** level is presented in electronic supplementary material, figure S2, and the dinitrogen evolution pathway of oxo-PZA is presented in figure 16. The determinant barrier concerned with the stability of oxo-PZA is 24.2 kcal mol^{-1}, which is comparable to that of PZA. The reactivity of oxo-PZA should be considered for further calculation. The reaction pathways for oxo-PZA and *m*-CPBA shown in figure 17 indicate that the oxygen atom of *m*-CPBA can attack the three different sites of oxo-PZA. The barriers for the formations of nitrite, 1,2-oxo-PZA and 1,3-oxo-PZA are 37.6, 23.9 and 20.6 kcal mol^{-1}, respectively. Therefore 1,3-oxo-PZA is the dominant production. The formation barrier of 1,3-oxo-PZA is also re-calculated at the RI-B2KPLYP/ma-def2-TZVP level, and the barrier is 25.8 kcal mol^{-1}. The dissociation of 1,3-oxo-PZA shown in figure 18 has a barrier of 22.7 kcal mol^{-1}. Compared with the computational results at the RI-B2KPLYP/ma-def2-TZVP and CCSD(T)/CBS levels, the calculation at the B3LYP/6-311++G** level underestimates the barrier to a certain degree. Consequently, the stabilities of oxo-PZA and 1,3-oxo-PZA are perhaps better. The synthesizabilities should be validated by further experimental studies.

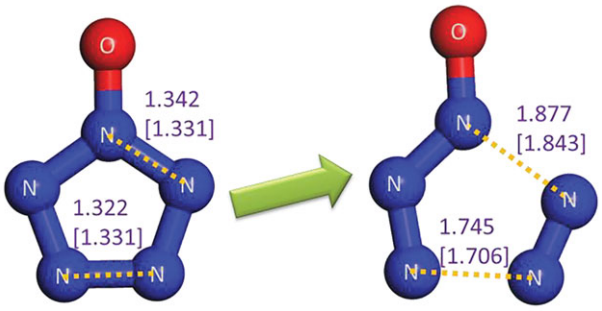

Figure 16. The determinant step for the dissociation of oxo-PZA. The system possesses one negative charge. The distances calculated at the B3LYP/6-311++G** and RI-B2KPLYP/ma-def2-TZVP (in parenthesis) levels are labelled in Å. The activation energy barrier including ZPC, activation enthalpy barrier at 298 K and activation free energy barrier at 298 K from complex of PZA and *m*-CPBA to TS are 25.0, 25.6 and 24.2 kcal mol^{-1} at the B3LYP/6-311++G** level, respectively, and 28.0, 28.5 and 27.4 kcal mol^{-1} at the RI-B2KPLYP/ma-def2-TZVP level, respectively. The activation energy barrier excluding ZPC at the CCSD(T)/CBS level is 33.3 kcal mol^{-1}.

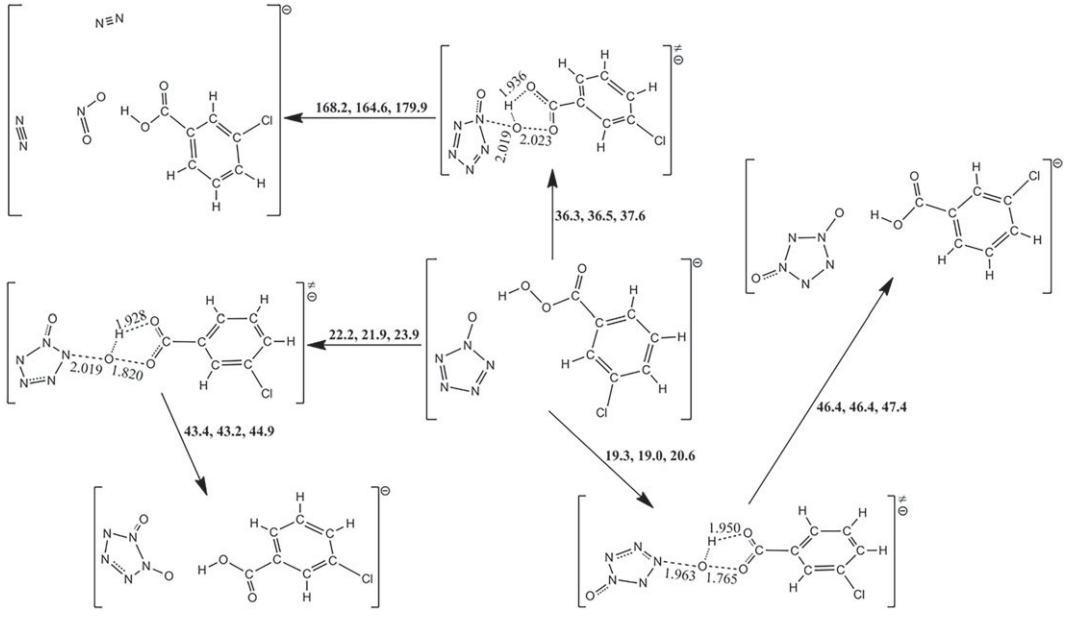

Figure 17. The PES scanning result for oxo-PZA and *m*-CPBA calculated at the B3LYP/6-311++G** level. The activation energy barriers (sum of total electronic energy and ZPC at front, enthalpy of 298 K at middle and free energy of 298 K at back) are in kcal mol^{-1}. The crucial bond lengths are labelled in Å.

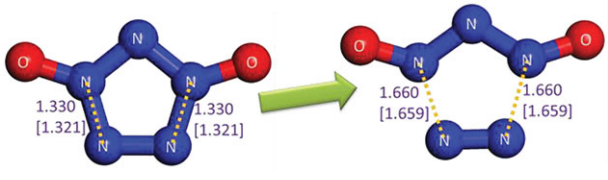

Figure 18. The process for dinitrogen evolution from 1,3-oxo-PZA to TS. The system possesses one negative charge. The distances calculated at the B3LYP/6-311++G** and RI-B2KPLYP/ma-def2-TZVP (in parenthesis) levels are labelled in Å. The activation energy barrier including ZPC, activation enthalpy barrier at 298 K and activation free energy barrier at 298 K from complex of PZA and *m*-CPBA to TS are 23.1, 23.5 and 22.7 kcal mol^{-1} at the B3LYP/6-311++G** level, respectively, and 28.0, 28.4 and 27.6 kcal mol^{-1} at the RI-B2KPLYP/ma-def2-TZVP level, respectively. The activation energy barrier excluding ZPC at the CCSD(T)/CBS level is 32.7 kcal mol^{-1}.

4. Conclusion

The synthetic and stable mechanisms for PZA have been credibly revealed by the quantum chemistry calculations on PESs. Although the mechanisms are not so perfect within the constraints of theoretical methods and computing resources, e.g. there is no interpretation of the source of ammonium, the

results presented in this paper have a valuable reference for illuminating the roads of theoretical and experimental studies on PZA. With the investigation above, we can draw conclusions as follows:

(1) Both singlet and triplet PPZ cannot produce PZA solely at ambient condition, because the processes are subject to the reaction thermodynamics. At high-energy condition, excitation of PPZ and deprotonation of PPZ-RA probably occur before the cleavage of C–N bond of PPZ.
(2) A new proton transfer pathway for the radical anion mechanism of PZA formation was found, but the pathway for the direct cleavage of C–N bond of PPZ-RA is still kinetically dominant. According to the verification of various methods, the barrier (about 25 kcal mol^{-1}) of PZA formation is close to that of dinitrogen evolution. Typically, the former is slightly lower than the latter at the CCSD(T)/CBS level. Even so, the ionic pair of sodium PPZ should be formed at a very low temperature, which is not beneficial in the reactivity. The endothermic process is another possible difficulty. The selection of other arylpentazole radical anions with large IPs should be focused in the subsequent experimental work. Moreover, due to the same level barriers for PZA formation and dissociation, the vigorous reaction condition is likely to cause the dinitrogen evolution.
(3) The direct cleavage of C–N bond of singlet PZPolA for PZA formation undergoes a MECP with an ultra-high effective barrier. The cleavage reaction between PZPolA and *m*-CPBA has a moderate barrier of about 20 kcal mol^{-1} which competes with the dinitrogen evolution of PZPolA. Although the reaction between PPZ and *m*-CPBA cannot form PZA, the reaction between PZPol and *m*-CPBA assisted by the proton absorption of glycinate anion can produce PZA with a barrier of about 20 kcal mol^{-1}. If the solvent effects are considered, the PZA formation starting with PZPolA is more feasible than that starting with PZPol.
(4) The ionic pair of $H_3O^+N_5^-$ is unstable. The proton can transfer to gaseous PZA without a barrier at high temperature, and then the hydrogenated pentazole exhausts dinitrogen, which is easier than PZA dissociation. The proton transfer in solid $(N_5)_6(H_3O)_3(NH_4)_4Cl$ can lead to concerted dissociation. The stability of solid $(N_5)_6(H_3O)_3(NH_4)_4Cl$ is better than that of gaseous PPZ.
(5) The quartet $Co(N_5)_2(H_2O)_4$, quintet $Fe(N_5)_2(H_2O)_4$ and sextet $Mn(N_5)_2(H_2O)_4$ are more thermodynamically stable than their low-spin states, which needs to be validated by the magnetic measurement. The Co coordination compound can spontaneously convert to the doublet $Co(N_5)(H_2O)_3{\cdot}H_2O$ at the high temperature. The quartet $Co(N_5)_2(H_2O)_2{\cdot}2H_2O$ is the most thermodynamically stable among $Co(N_5)_2(H_2O)_n{\cdot}$ (4-n)H_2O. The exposed pentazolyl group in $Co(N_5)_2(H_2O)_2{\cdot}2H_2O$ is less kinetically stable than that confined by the crystal waters. If the confined effect is taken into account, the coordinate compound with the pentazolyl groups is still less kinetically stable than gaseous PZA. According to the computational result of similar reactions, $Fe(N_5)_2(H_2O)_4$ and $Mn(N_5)_2(H_2O)_4$ are more stable than $Co(N_5)_2(H_2O)_4$.
(6) PZA can be persistently oxidized by *m*-CPBA to oxo-PZA and 1,3-oxo-PZA. The reactivity of *m*-CPBA with PZA is almost the same as those with PZPolA and PZPol. The selectivity of *m*-CPBA and synthetic method of oxo-PZA must be explained by both experimental and theoretical efforts in the future.

Data accessibility. Electronic supplementary material is available on Figshare. The *xyz* coordinates for the optimized geometries and their total energies, the computational test of different quantum chemistry methods on dissociation barriers, the solvent effect for radical anion mechanism, the PES scanning result for *m*-chloroperbenzoic acid (*m*-CPBA), the PES scanning result for oxo-phenylpentazole (oxo-PPZ) and the crystallographic information file for the TS of the solid $(N_5)_6(H_3O)_3(NH_4)_4Cl$ dissociation.

Authors' contributions. T.Y. managed the research. Y.-D.M, W.-P.L., Y.-Z.L., Z.-X.G. and G.R. assisted with calculation and data analysis. T.Y. and Y.-D.M wrote the manuscript. W.-P.L., Y.-Z.L., Z.-X.G. and G.R. revised the manuscript.

Competing interests. We have no competing interests.

Funding. The work presented here and all authors were funded by the National Natural Science Foundation of China (nos. 21403162 and 21503160).

Acknowledgements. We thank Dr Bai-Sheng Sa of Fuzhou University for his supercomputing resource.

References

1. Curtius T. 1890 Ueber Stickstoffwasserstoffsäure (Azoimid) N_3H. *Ber. Dtsch. Chem. Ges.* **23**, 3023–3033. (doi:10.1002/cber.18900230232)
2. Christe KO, Wilson WW, Sheehy JA, Boatz JA. 1999 N_5^+: a novel homoleptic polynitrogen ion as a high energy density material. *Angew. Chem. Int. Ed.* **38**, 2004–2009. (doi:10.1002/(SICI)1521-3773(19990712)38:13/14<2004::AID-ANIE2004>3.0.CO;2-7)
3. Ugi I. 1964 Pentazoles. *Adv. Heterocycl. Chem.* **3**, 373–383. (doi:10.1016/S0065-2725(08)60546-2)

4. Curtiss LA, Raghavachari K, Redfern PC, Pople JA. 1997 Assessment of Gaussian-2 and density functional theories for the computation of enthalpies of formation. *J. Chem. Phys.* **103**, 1063–1079. (doi:10.1063/1.473182)
5. Nguyen MT, Hab T-K. 2000 Theoretical study of the pentanitrogen cation (N_5^+). *Chem. Phys. Lett.* **317**, 135–141. (doi:10.1016/S0009-2614(99)01320-2)
6. Dixon DA, Feller D, Christe KO, Wilson WW, Vij A, Vij V, Jenkins HDB, Olson RM, Gordon MS. 2004 Enthalpies of formation of gas-phase N_3, N_3^-, N_5^+, and N_5^- from ab initio molecular orbital theory, stability predictions for $N_5^+N_3^-$ and $N_5^+N_5^-$, and experimental evidence for the instability of $N_5^+N_3^-$. *J. Am. Chem. Soc.* **126**, 834–843. (doi:10.1021/ja0303182)
7. Vij A, Pavlovich JG, Wilson WW, Vij V, Christe KO. 2002 Experimental detection of the pentaazacyclopentadienide (pentazolate) anion, *cyclo*-N_5^-. *Angew. Chem. Int. Ed.* **41**, 3051–3054. (doi:10.1002/1521-3773(20020816)41:16<3051::AID-ANIE3051>3.0.CO;2-T)
8. Belau L, Haas Y, Zilberg S. 2004 Formation of the *cyclo*-pentazolate N_5^- anion by high-energy dissociation of phenylpentazole anions. *J. Phys. Chem. A* **108**, 11 715–11 720. (doi:10.1021/jp046905 7)
9. Östmark H, Wallin S, Brink T, Carlqvist P, Claridge R, Hedlund E, Yudina L. 2003 Detection of pentazolate anion (*cyclo*-N_5^-) from laser ionization and decomposition of solid *p*-dimethylaminophenylpentazole. *Chem. Phys. Lett.* **379**, 539–546. (doi:10.1016/j.cplett.2003.08.081)
10. Bazanov B, Geiger U, Carmieli R, Grinstein D, Welner S, Haas Y. 2016 Detection of cyclo-N_5^- in THF solution. *Angew. Chem. Int. Ed.* **55**, 13 233–13 235. (doi:10.1002/anie.201605400)
11. Geiger U, Haas Y. 2016 Preparation of the cyclopentazole anion in the bulk: a computational study. *J. Phys. Chem. B* **120**, 6208–6214. (doi:10.1021/acs.jpcb.6b02228)
12. Bazanov B, Geiger U, Grinstein D, Welner S, Haas Y. 2017 N_5^- in solution: isotopic labeling and further details of its synthesis by phenyl pentazole reduction. *J. Phys. Chem. A* **121**, 6727–6731. (doi:10.1021/acs.jpca.7b04222)
13. Steele B, Stavrou E, Crowhurst JC, Zaug JM, Prakapenka VB, Oleynik II. 2017 High-pressure synthesis of a pentazolate salt. *Chem. Mater.* **29**, 735–741. (doi:10.1021/acs.chemmater.6b04538)
14. Laniel D, Weck G, Gaiffe G, Garbarino G, Loubeyre P. 2018 High-pressure synthesized lithium pentazolate compound metastable under ambient conditions. *J. Phys. Chem. Lett.* **9**, 1600–1604. (doi:10.1021/acs.jpclett.8b00540)
15. Butler RN, Stephens JC, Burke LA. 2003 First generation of pentazole (HN_5, pentazolic acid), the final azole, and a zinc pentazolate salt in solution: a new *N*-dearylation of 1-(*p*-methoxyphenyl) pyrazoles, a 2-(*p*-methoxyphenyl) tetrazole and application of the methodology to 1-(*p*-methoxyphenyl) pentazole. *Chem. Commun.* **2003**, 1016–1017. (doi:10.1039/B301491F)
16. Schroer T, Haiges R, Schneider S, Christe KO. 2005 The race for the first generation of the pentazolate anion in solution is far from over. *Chem. Commun.* **2005**, 1607–1609. (doi:10.1039/B417010E)
17. Butler RN, Hanniffy JM, Stephens JC, Burke LA. 2008 A ceric ammonium nitrate N-dearylation of *N*-*p*-anisylazoles applied to pyrazole, triazole, tetrazole, and pentazole rings: release of parent azoles. Generation of unstable pentazole, HN_5/N_5^-, in solution. *J. Org. Chem.* **73**, 1354–1364. (doi:10.1021/jo702423z)
18. Perera SA, Gregušová A, Bartlett RJ. 2009 First calculations of $^{15}N—^{15}N$ *J* values and new calculations of chemical shifts for high nitrogen systems: a comment on the long search for HN_5 and its pentazole anion. *J. Phys. Chem. A* **113**, 3197–3201. (doi:10.1021/jp809267y)
19. Zhang C, Sun C, Hu B, Yu C, Lu M. 2017 Synthesis and characterization of the pentazolate anion *cyclo*-N_5^- in $(N_5)_6(H_3O)_3(NH_4)_4Cl$. *Science* **355**, 374–376. (doi:10.1126/science.aah3840)
20. Zhang C, Yang C, Hu B, Yu C, Zheng Z, Sun C. 2017 A symmetric $Co(N_5)_2(H_2O)_4 \cdot 4H_2O$ high-nitrogen compound formed by cobalt(II) cation trapping of a cyclo-N_5^- anion. *Angew. Chem. Int. Ed.* **56**, 4512–4514. (doi:10.1002/anie.201701070)
21. Zhang W, Wang K, Li J, Lin Z, Song S, Huang S, Liu Y, Nie F, Zhang Q. 2018 Stabilization of the pentazolate anion in a zeolitic architecture with $Na_{20}N_{60}$ and $Na_{24}N_{60}$ nanocages. *Angew. Chem. Int. Ed.* **57**, 2592–2595. (doi:10.1002/anie.201710602)
22. Sun C, Zhang C, Jiang C, Yang C, Du Y, Zhao Y, Hu B, Zheng Z, Christe KO. 2018 Synthesis of AgN_5 and its extended 3D energetic framework. *Nat. Commun.* **9**, 1269. (doi:10.1038/s41467-018-03678-y)
23. Xu Y, Wang Q, Shen C, Lin Q, Wang P, Lu M. 2017 A series of energetic metal pentazolate hydrates. *Nature* **549**, 78–81. (doi:10.1038/nature23662)
24. Xu Y, Lin Q, Wang P, Lu M. 2018 Stabilization of the pentazolate anion in three anhydrous and metal-free energetic salts. *Chem. Asian J.* **13**, 924–928. (doi:10.1002/asia.201800187)
25. Xu W-G, Li G-L, Wang L-J, Li S, Li Q-S. 1999 Ab initio and density functional theory study of the mechanism of synthesis of the N_5^+ cation. *Chem. Phys. Lett.* **314**, 300–306. (doi:10.1016/S0009-2614(99)01164-1)
26. Yu T, Liu Y-Z, Haiges R, Christe KO, Lai W-P, Wu B. 2014 4-Oxo- or 1-oxo-N70–+? A computational and experimental study. *RSC Adv.* **4**, 28 377–28 389. (doi:10.1039/C4RA02140A)
27. Wilson WW, Haiges R, Boatz JA, Christe KO. 2007 Synthesis and characterization of (*Z*)-$[N_3NFO]^+$ and (*E*)-$[N_3NFO]^+$. *Angew. Chem. Int. Ed.* **46**, 3023–3027. (doi:10.1002/anie.200700130)
28. Christe KO, Haiges R, Wilson WW, Boatz JA. 2010 Synthesis and properties of N_7O^+. *Inorg. Chem.* **49**, 1245–1251. (doi:10.1021/ic9022213)
29. Becke AD. 1993 Density-functional thermochemistry. III. The role of exact exchange. *J. Chem. Phys.* **98**, 5648–5652. (doi:10.1063/1.464913)
30. Lee C, Yang W, Parr RG. 1988 Development of the Colle-Salvetti correlation-energy formula into a functional of the electron density. *Phys. Rev. B* **37**, 785–789. (doi:10.1103/PhysRevB.37.785)
31. Tarnopolsky A, Karton A, Sertchook R, Vuzman D, Martin JML. 2008 Double-hybrid functionals for thermochemical kinetics. *J. Phys. Chem. A* **112**, 3–8. (doi:10.1021/jp710179r)
32. Grimme S. 2006 Semiempirical hybrid density functional with perturbative second-order correlation. *J. Chem. Phys.* **124**, 034108. (doi:10.1063/1.2148954)
33. Weigend F, Häser M. 1997 RI-MP2: first derivatives and global consistency. *Theor. Chem. Acc.* **97**, 331–340. (doi:10.1007/s002140050269)
34. Cizek J. 2007 On the use of the cluster expansion and the technique of diagrams in calculations of correlation effects in atoms and molecules. In *Advances in chemical physics* (eds R LeFebvre, C Moser), pp. 35–89. Hoboken, NJ: John Wiley & Sons, Inc.
35. Purvis III GD, Bartlett RJ. 1982 A full coupled-cluster singles and doubles model: the inclusion of disconnected triples. *J. Chem. Phys.* **76**, 1910–1918. (doi:10.1063/1.443164)
36. Scuseria GE, Janssen CL, Schaefer III HF. 1988 An efficient reformulation of the closed-shell coupled cluster single and double excitation (CCSD) equations. *J. Chem. Phys.* **89**, 7382–7387. (doi:10.1063/1.455269)
37. Scuseria GE, Schaefer III HF. 1989 Is coupled cluster singles and doubles (CCSD) more computationally intensive than quadratic configuration interaction (QCISD)? *J Chem. Phys.* **90**, 3700–3703. (doi:10.1063/1.455827)
38. Pople JA, Head-Gordon M, Raghavachari K. 1987 Quadratic configuration interaction: a general technique for determining electron correlation energies. *J. Chem. Phys.* **87**, 5968–5975. (doi:10.1063/1.453520)
39. Krishnan R, Binkley JS, Seeger R, Pople JA. 1980 Self-consistent molecular orbital methods. XX. A basis set for correlated wave functions. *J. Chem. Phys.* **72**, 650–654. (doi:10.1063/1.438955)
40. Hay PJ, Wadt WR. 1985 Ab initio effective core potentials for molecular calculations: potentials for the transition metal atoms Sc to Hg. *J. Chem. Phys.* **82**, 270–283. (doi:10.1063/1.448799)
41. Hay PJ, Wadt WR. 1985 Ab initio effective core potentials for molecular calculations: potentials for K to Au including the outermost core orbitals. *J. Chem. Phys.* **82**, 299–310. (doi:10.1063/1.448975)
42. Weigend F, Ahlrichs R. 2005 Balanced basis sets of split valence, triple zeta valence and quadruple zeta valence quality for H to Rn: design and assessment of accuracy. *Phys. Chem. Chem. Phys.* **7**, 3297–3305. (doi:10.1039/B508541A)
43. Zheng J, Xu X, Truhlar DG. 2011 Minimally augmented Karlsruhe basis sets. *Theor. Chem. Acc.* **128**, 295–305. (doi:10.1007/s00214-010-0846-z)
44. Truhlar DG. 1998 Basis-set extrapolation. *Chem. Phys. Lett.* **294**, 45–48. (doi:10.1016/S0009-2614(98)00866-5)
45. Dunning Jr TH. 1989 Gaussian basis sets for use in correlated molecular calculations. I. The atoms boron through neon and hydrogen. *J. Chem. Phys.* **90**, 1007–1023. (doi:10.1063/1.456153)
46. Frisch MJ *et al.* 2009 *Gaussian 09, Revision B. 01*. Wallingford, CT: Gaussian, Inc.
47. Neese F. 2012 The ORCA program system. *WIREs Comput. Mol. Sci.* **2**, 73–78. (doi: 10.1002/wcms.81)
48. Tomasi J, Mennucci B, Cammi R. 2005 Quantum mechanical continuum solvation models. *Chem. Rev.* **105**, 2999–3094. (doi:10.1021/cr9904009)
49. Tomasi J, Mennucci B, Cancès E. 1999 The IEF version of the PCM solvation method: an overview of a new method addressed to study molecular solutes at the QM ab initio level. *J. Mol. Struct. Theochem* **464**, 211–226. (doi:10.1016/S0166-1280(98)00553-3)
50. Scalmani G, Frisch MJ. 2010 Continuous surface charge polarizable continuum models of solvation.

I. General formalism. *J. Chem. Phys.* **132**, 114110. (doi:10.1063/1.3359469)

51. Jenkins HDB, Roobottom HK, Passmore J, Glasser L. 1999 Relationships among ionic lattice energies, molecular (formula unit) volumes, and thermochemical radii. *Inorg. Chem.* **38**, 3609–3620. (doi:10.1021/ic9812961)
52. Perdew JP, Burke K, Ernzerhof M. 1996 Generalized gradient approximation made simple. *Phys. Rev. Lett.* **77**, 3865–3868. (doi:10.1103/PhysRevLett.77.3865)
53. Perdew JP, Burke K, Ernzerhof M. 1997 Errata: generalized gradient approximation made simple. *Phys. Rev. Lett.* **78**, 1396. (doi:10.1103/PhysRevLett.78.1396)
54. Vanderbilt D. 1990 Soft self-consistent pseudopotentials in a generalized eigenvalue formalism. *Phys. Rev. B* **41**, 7892–7895. (doi:10.1103/PhysRevB.41.7892)
55. Segall MD, Probert MJ, Pickard CJ, Hasnip PJ, Clark SJ, Refson K, Yates JR, Payne MC. 2000–2014 *Materials studio CASTEP version 8.0*. Cambridge, UK: Cambridge University and Accelrys Inc.
56. Tkatchenko A, Scheffler M. 2009 Accurate molecular van der Waals interactions from ground-state electron density and free-atom reference data. *Phys. Rev. Lett.* **102**, 073005. (doi:10.1103/PhysRevLett.102.073005)
57. Clark SJ, Segall MD, Pickard CJ, Hasnip PJ, Probert MIJ, Refson K, Payne MC. 2005 First principles methods using CASTEP. *Z. Kristallogr.* **220**, 567–570. (doi:10.1524/zkri.220.5.567.65075)
58. Butler RN, Fox A, Collier S, Burke LA. 1998 Pentazole chemistry: the mechanism of the reaction of aryldiazonium chlorides with azide ion at −80 C: concerted versus stepwise formation of arylpentazoles, detection of a pentazene intermediate, a combined ^{1}H and ^{15}N NMR experimental and *ab initio* theoretical study. *J. Chem. Soc. Perkin Trans.* **2**, 2243–2248. (doi:10.1039/A804040K)
59. Burke LA, Fazen PJ. 2009 Correlation analysis of the interconversion and nitrogen loss reactions of aryl pentazenes and pentazoles derived from aryl diazonium and azide ions. *Int. J. Quantum Chem.* **109**, 3613–3618. (doi:10.1002/qua.22408)
60. Lide DR. 2003–2004 *CRC handbook of chemistry and physics*, 84th edn. Boca Raton, FL: CRC Press.
61. Hammerl A, Klapötke TM, Schwerdtfeger P. 2003 Azolylpentazoles as high-energy materials: a computational study. *Chem. Eur. J.* **9**, 5511–5519. (doi:10.1002/chem.200305125)
62. Rahm M, Brinck T. 2010 Kinetic stability and propellant performance of green energetic materials. *Chem. Eur. J.* **16**, 6590–6600. (doi:10.1002/chem.201000413)